AGU PUBLICATIONS

JGR

Journal of Geophysical Research: Solid Earth

RESEARCH ARTICLE
10.1002/2014JB010982

Key Points:
- The ascent of magma beneath Azores mainly focused over localized melting sources
- Dykes propagate laterally in upper levels of the crust from the magma chambers
- AMS data allow the calculation of magmatic flow vectors in dikes from the Azores

Correspondence to:
M. A. Moreira,
mmoreira@adf.isel.pt

Citation:
Moreira, M. A., L. Geoffroy, and J. P. Pozzi (2015), Magma flow pattern in dykes of the Azores revealed by anisotropy of magnetic susceptibility, *J. Geophys. Res. Solid Earth*, *120*, 662–690, doi:10.1002/2014JB010982.

Received 23 JAN 2014
Accepted 26 NOV 2014
Accepted article online 5 DEC 2014
Published online 17 FEB 2015

Magma flow pattern in dykes of the Azores revealed by anisotropy of magnetic susceptibility

M. A. Moreira[1,2], L. Geoffroy[3], and J. P. Pozzi[4]

[1]Instituto Superior de Engenharia de Lisboa, Lisboa, Portugal, [2]Instituto Dom Luís, Lisboa, Portugal, [3]Laboratoire Domaines Océaniques, CNRS (UMR 6538), Institut Universitaire Européen de la Mer, Université de Brest, Plouzané, France, [4]Laboratoire de Géologie, CNRS (UMR 8538), École Normale Supérieure, Paris, France

Abstract The localization of magma melting areas at the lithosphere bottom in extensional volcanic domains is poorly understood. Large polygenetic volcanoes of long duration and their associated magma chambers suggest that melting at depth may be focused at specific points within the mantle. To validate the hypothesis that the magma feeding a mafic crust, comes from permanent localized crustal reservoirs, it is necessary to map the fossilized magma flow within the crustal planar intrusions. Using the AMS, we obtain magmatic flow vectors from 34 alkaline basaltic dykes from São Jorge, São Miguel and Santa Maria islands in the Azores Archipelago, a hot-spot related triple junction. The dykes contain titanomagnetite showing a wide spectrum of solid solution ranging from Ti-rich to Ti-poor compositions with vestiges of maghemitization. Most of the dykes exhibit a normal magnetic fabric. The orientation of the magnetic lineation k_1 axis is more variable than that of the $k3$ axis, which is generally well grouped. The dykes of São Jorge and São Miguel show a predominance of subhorizontal magmatic flows. In Santa Maria the deduced flow pattern is less systematic changing from subhorizontal in the southern part of the island to oblique in north. These results suggest that the ascent of magma beneath the islands of Azores is predominantly over localized melting sources and then collected within shallow magma chambers. According to this concept, dykes in the upper levels of the crust propagate laterally away from these magma chambers thus feeding the lava flows observed at the surface.

1. Introduction

1.1. Magmatism at Divergent Plate Boundaries

While oceanic spreading ridges are fundamentally segmented along strike, the wavelength and nature of this segmentation differs depending upon the ridge spreading rate [e.g., *Macdonald et al.,* 1988]. At slow-spreading ridges, accretion segments define the first-order segmentation [*Durand et al.,* 1995; *Gente et al.,* 1995, 2003; *Lin et al.,* 1990]. The center of these segments is associated with a central volcanic area where most of the volcanic and hydrothermal activities are observed, bounded on either side by fault-controlled deeper basins. As *Tolstoy et al.* [1993] clearly outlined, the crust thickness is higher at the segment center where most of the volcanic activity is observed and where tectonic extension dominates over magma accretion/dilatation. Analogous volcano-tectonic segments are found in other geodynamical contexts such as volcanic rifts in continental Large Igneous Provinces (LIP) [*Geoffroy et al.,* 2007] where a hot spot is interacting dynamically and magmatically with a nascent ridge, e.g., Djibouti [see *De Chabalier and Avouac*, 1994], or an established slow-spreading ridge (e.g., Iceland). In these latter cases, the central magmatic activity is expressed by a large polygenetic volcano, underlain by one or several large magma chambers located at shallow levels (3–5 km) [e.g., *Bjornsson et al.*, 1979; *Paquet et al.*, 2007]. A very common observation in fossilized or active volcano-tectonic segments is that the magma chambers, underlying the central volcanic system, feeds lava fields through lateral and radial propagated dykes at the extremities of the segment (Figure 1). Following from the model of *Chevalier and Verwoerd* [1988], *Geoffroy* [1998] and *Doubre and Geoffroy* [2003] argued that this mechanism is potentially viable because magma chambers act as stress concentrators within the upper crust. According to these authors, dykes develop preferentially from the edges of magma chambers along the horizontal maximum stress σ_H. Only high magma pressures or/and small stress differential in the horizontal plane could promote a more radial pattern of dykes injection. From a review of previous studies of magma flow in dykes including eroded and active extensional systems, *Geoffroy et al.* [2007] suggest that magma is injected laterally in dykes within the upper crust (for a review of more recent data, see *Wright et al.* [2012]).

©2014. American Geophysical Union. All Rights Reserved.

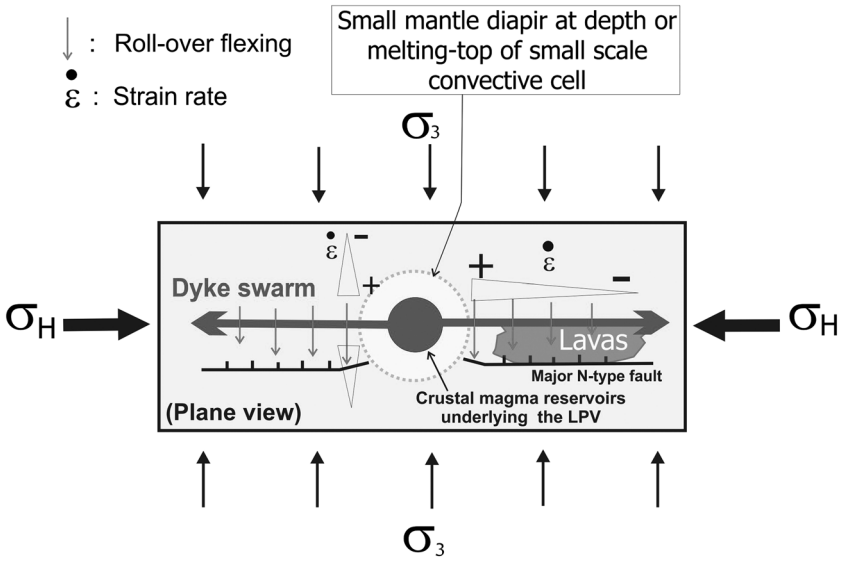

Figure 1. Conceptual model of volcano-tectonic segment in a horizontal plane view after *Geoffroy* [2005]. Upper crustal magma reservoirs (magma chambers) are located beneath a large polygenetic volcano or a central volcano-tectonic system, not represented in the figure. These crustal reservoirs are fed directly or indirectly by the magma extracted from a localized melting zone at the asthenosphere-lithosphere boundary. This mantle zone may either correspond to the upper part of a small-scale convection cell [*Geoffroy et al.,* 2007] or a mantle diapir [*Geoffroy*, 1998; *Burg et al.,* 2009]. The upper magma reservoirs are subject to hydraulic-type fracturing due to stress concentration at their edges, thus promoting dyke injection in the trend of the maximum horizontal compressive stress σ_H. These dykes feed the upper crust producing lava flows and tuffs when crosscutting the ground surface. In addition, the asthenospheric localized instability generates high thermal gradients at the center of the volcano-tectonic segment, which favors the development of tectonic extension in the upper crust [see *Callot et al*., 2001]. Thin triangles along and normal to σ_H represent the relative elongation and shortening direction.

These views conflict with old conceptual models, suggesting that the dynamics of magma could be dominantly bottom to top from "deep magma layers" [e.g., *Gudmundsson* 1986, 1990]. *Geoffroy* [2005] and *Geoffroy et al.* [2007] indicate the geodynamical importance of this result: if most of the lavas at spreading ridges and in LIPs are fed from dykes issued from long-lived magma centers and crosscutting the topographic surface, this gives some insights into the distribution of melting at the asthenosphere-lithosphere boundary [see *Geoffroy et al*., 2007, and references therein]. Figure 1 summarizes the generalized LIP accretion segment concept developed by *Geoffroy et al.* [2007]: the upper crustal magma reservoir underlying each volcano segment center is directly or indirectly fed by the development of either a mantle diapir [*Geoffroy*, 1998] or a small-scale convection cell [*Geoffroy et al.,* 2007]. This mantle upwelling thermally weakens the lithosphere, creating a so-called lithospheric (rheological) soft point [e.g., *Callot and Geoffroy,* 2004; *Gac and Geoffroy*, 2005]. In addition, this lithosphere-scale weakening leads to a lithosphere stretching and thinning that is orthogonal to the regional minimum principal stress $\sigma 3$ and in the trend of the maximum horizontal stress σ_H (intersection of the $\sigma 1$-$\sigma 2$ plane with the topographic surface). Moreover, the upper crustal magma chambers act as local stress concentrators, promoting dykes injection orthogonal to $\sigma 3$ and in the trend of σ_H. As a result, within the upper crust, the active normal faults are focused away from the magma center and control the subsidence and topography of basins in which the magma flows from the intersection of dikes with the topographic surface.

Such views, which have important consequences on the way we understand mantle melting processes, remain to be validated. Therefore, it is important to have additional constraints on the pattern of magma flow and crustal growth in divergent magmatic systems, especially in contexts where the dynamics of the mantle is thought to be complex (e.g., oceanic ridge/hot spot interaction).

Our study is focused on the determination of magma flow vectors in the upper crust of a particular complex volcano-tectonic setting, the Azores hot spot.

©2014. American Geophysical Union. All Rights Reserved.

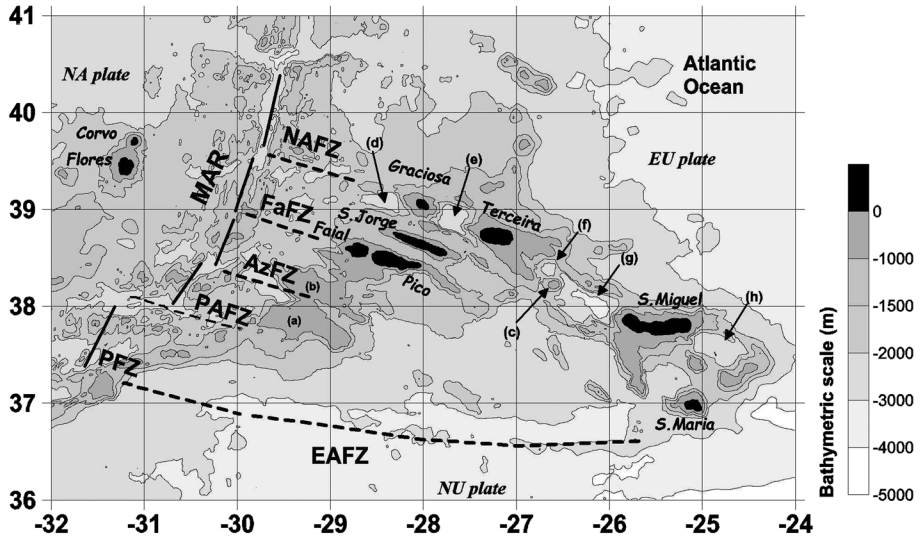

Figure 2. Simplified bathymetry of Azores Plateau and main tectonic features, contoured at 1000 m interval based on *Luís et al.* [1994] and *Lourenço et al.* [1998]. Latitude and longitude in degrees are indicated along the margins. Legend: NA plate: North Atlantic Plate; EU plate: Eurasian Plate; NU plate: Nubian Plate; MAR: Mid-Atlantic Ridge; NAFZ: North Azores Fracture Zone; FaFZ: Faial Fracture Zone; AzFZ: Azor Fracture Zone; PAFZ: Princess Alice Fracture Zone; PFZ: Pico Fracture Zone; EAFZ: East Azores Fracture Zone. (a) Princess Alice bank; (b) Azor bank; (c) Dom João de Castro bank; (d) West Graciosa Basin; (e) East Graciosa Basin; (f) North Hirondelle Basin; (g) South Hirondelle Basin; and (h) Povoação Basin.

1.2. The Azores Area: A Combination Between a Hot Spot and a Triple Junction

The Azores region consists broadly of a triangular anomalous shallow volcanic plateau centered to the east of the Mid-Atlantic Ridge (Figure 2). To the northeast of this plateau, the en echelon Terceira and Faial-Pico rift system (here designated as the Terceira Rift System, TRS) form a seismically active 125° azimuth trending divergent plate boundary between Africa and Eurasia with a present-day half-spreading rate of ~2.5 mm/yr along 063° trend [*De Mets et al.,* 1990; *Luis et al.,* 1989; *Luis and Miranda*, 2008]. Together with the Middle Atlantic Ridge (MAR) north and south of latitude ~39°N, the TRS would be the third rift arm of a Ridge-Ridge-Ridge or Ridge-transform Fault-transform Fault triple junction between the North American, Eurasia, and Africa Plates [e.g., *Searle*, 1980]. A curious set of en echelon abandoned volcanic ridges trending parallel to the TRS extends from the extinct East Azores Fault Zone to the south of the plateau to the active TRS, from south to north: Princess Alice Bank, Azores Bank, Terra-San Mateus Bank (Figure 2). This could suggest a progressive northward migration of the triple junction, as formerly suggested by *McKenzie and Morgan* [1969], a view contradicted by *Searle* [1980] but rejuvenated by *Luís et al.* [1994]. Alternatively, this pattern could suggest a southwestward absolute migration of the Africa-Eurasia Plates over a fixed hot spot now located close to the Terceira Island [e.g., *Yang et al.,* 2006].

Recent studies involving elastic plate modeling [*Luis et al.,* 1998; *Luis and Neves*, 2006] point to a mean crust thickness of about 9–12 km for the Azores Plateau. This excess in oceanic crustal thickness suggests that the Azores Plateau is located above a subsolidus mantle. Trace elements and helium and lead isotope geochemistry suggest that the extreme variability in composition of the mantle source beneath the Azores Archipelago [e.g., *Bonati,* 1990; *Moreira et al.,* 1999a; *Dosso et al.,* 1999; *Schaefer et al.,* 2002; *Widom and Farquhar,* 2003; *Asimow and Langmuir,* 2003]. These data indicate that the mantle is fertile, rich in radiogenic elements, but evidence is lacking from the geochemistry for a deep mantle plume. A seismic study of the mantle beneath Azores led *Yang et al.* [2006] to a model of a plume-ridge interaction, in which the plume conduit is deflected to the southwest in the shallow mantle by asthenospheric flow and plate motion. Anisotropic surface waves tomographic studies [*Silveira et al.,* 2006] revealed an *S* wave velocity negative anomaly beneath Azores, confined within the upper 250–300 km, pointing to the hypothesis that Azores could be a present-day dying plume.

The origin of the Azores Plateau remains unclear. Continental mantle lithosphere contributions have been invoked [*Dosso et al.,* 1999; *Moreira et al.,* 1999a] and the imaging of a deep mantle plume is still a matter of debate. It is clear, however, that a large mantle compositional anomaly is present beneath the plateau [see

©2014. American Geophysical Union. All Rights Reserved.

also *Vlastélic et al.,* 2002]. Whatever its origin, it must be kept in mind that the tectonic expression and the regional tensional regime of the Azores dynamics control the magmatic feeding and form a diffuse plate boundary that weakly overprint the MAR's spreading seafloor. This is particularly evident from magnetic and gravity data [*Lourenço et al.,* 1998].

1.3. Volcano-Tectonic Features of the TRS and Aim of the Study

The TRS (including Faial and Pico alignments) is a seismically and volcanically active ~120° trending structure. It shows an alternating morphology between the islands represented by bathymetric highs and the offshore deep basins (Figure 2). Most islands and deeps present a noncircular outer shape with a long axis generally parallel to the overall ~110° to 125° azimuth trend. Each TRS island is associated with one or several large polygenic volcanoes and subordinated alignments of fissure-borne monogenic cones. No TRS alkaline volcanism is older than 4 Ma (at the eastern edge of San Miguel Island), and the bulk of it is younger than 1.3 Ma [*Feraud et al.,* 1980; *Luís et al.,* 1994; *Hildenbrand et al.,* 2008].

The overall organization of the TRS could suggest that this rift is a very recent oceanic ultraslow-spreading axis consisting of distinct volcano-tectonic segments (Figure 1). The narrowness of the spreading axis is outlined by the pattern of the pre–hot spot MAR-related linear magnetic anomalies, which are still recognizable very close to the islands [*Luis et al.,* 1989] and by the distribution of the seismicity. The islands broadly correspond to the volcanic centers, whereas lateral deeps could be areas from apart the magma centers where divergence takes place predominantly by tectonic extension rather than magmatic accretion. This overall structure is suggested by the pattern of volcanism and deformation. Point-source volcanism is suggested by the associated occurrence of large polygenic volcanoes and the important role of fissural volcanism. Fissural volcanism is characterized by alignments of monogenetic cones and the exposure of dyke swarms in eroded cliffs, being generally centered on the polygenetic volcanoes. Significantly, the eruptive fissures are roughly parallel to the general alignments of the segments forming the TRS, except notably on Santa Maria (Figure 3). In addition, while normal faults are the dominant pattern of faulting on the islands [*Hildenbrand et al.,* 2012] there is, nevertheless, a clear component of dextral shear [*Searle,* 1980]. The normal faults are best developed at the NW and SE edges of the islands, with throws increasing toward the offshore basins. This is consistent with the distribution of seismicity, which is preferentially located between the volcanic centers [*Miranda et al.,* 1998]. These rift-type trends dominantly parallel to the dyke swarms with fissural volcanism at the ground surface.

However, this general volcano-tectonic segmentation proposed for the structure of the TRS is challenged by a number of additional facts and observations which must be taken into account. Although rather few focal mechanisms are published for seismic events in the Azores, extensional double couple is expressed along the TRS [*Grimison and Chen*, 1986] with *P* axes generally plunging with a significant dip [*Buforn et al*., 1988; *Hirn et al.,* 1980]. It is noteworthy that the solution for the last major earthquake (January 1980, $M \sim 7$) and its aftershocks indicates a sinistral strike-slip displacement along a 154° azimuth fault between São Jorge and Terceira islands [*Hirn et al.,* 1980]. Therefore, in the tectonic setting of the TRS, we must consider the consequence of the obliquity of the volcano-tectonic rift system in relation to the present-day kinematic vector between the Eurasia and Africa Plates. This obliquity would generate a component of dextral shear along the plate boundary that probably promotes some bookshelf faulting and vertical axis rotation between the islands [*Hirn et al.,* 1993; *Miranda et al.,* 1998].

Another important point is the geodynamical setting of the São Jorge and Santa Maria islands. São Jorge is located between the overlapping axis of Faial-Pico and the Terceira rift and consists of a linear volcanic ridge whose topography is dominated by a chain of monogenetic volcanic cones trending ~120°. This direction is also apparent in the dykes from the oldest part of the island [*Moreira et al.,* 1999b; *Hildenbrand et al.,* 2008]. No igneous centers are observed on São Jorge in contrast with the other TRS islands. Santa Maria occupies a southerly position in relation to the TRS and EUR/AFR plate boundary (Figure 2). The lava flows are older than elsewhere with maximum ages of 8.12 Ma [*Feraud et al.,* 1980] and this seismically inactive island lies at the eastern edge of the inactive East Azores Fracture Zone. The island is associated with a particular configuration of dykes with an apparent radial pattern at the scale of the island.

In this study, we present the deduced orientation of the fossilized magma flow vectors derived from dykes sampled from the islands of São Jorge, São Miguel and Santa Maria. In addition to observing the geometry of

©2014. American Geophysical Union. All Rights Reserved.

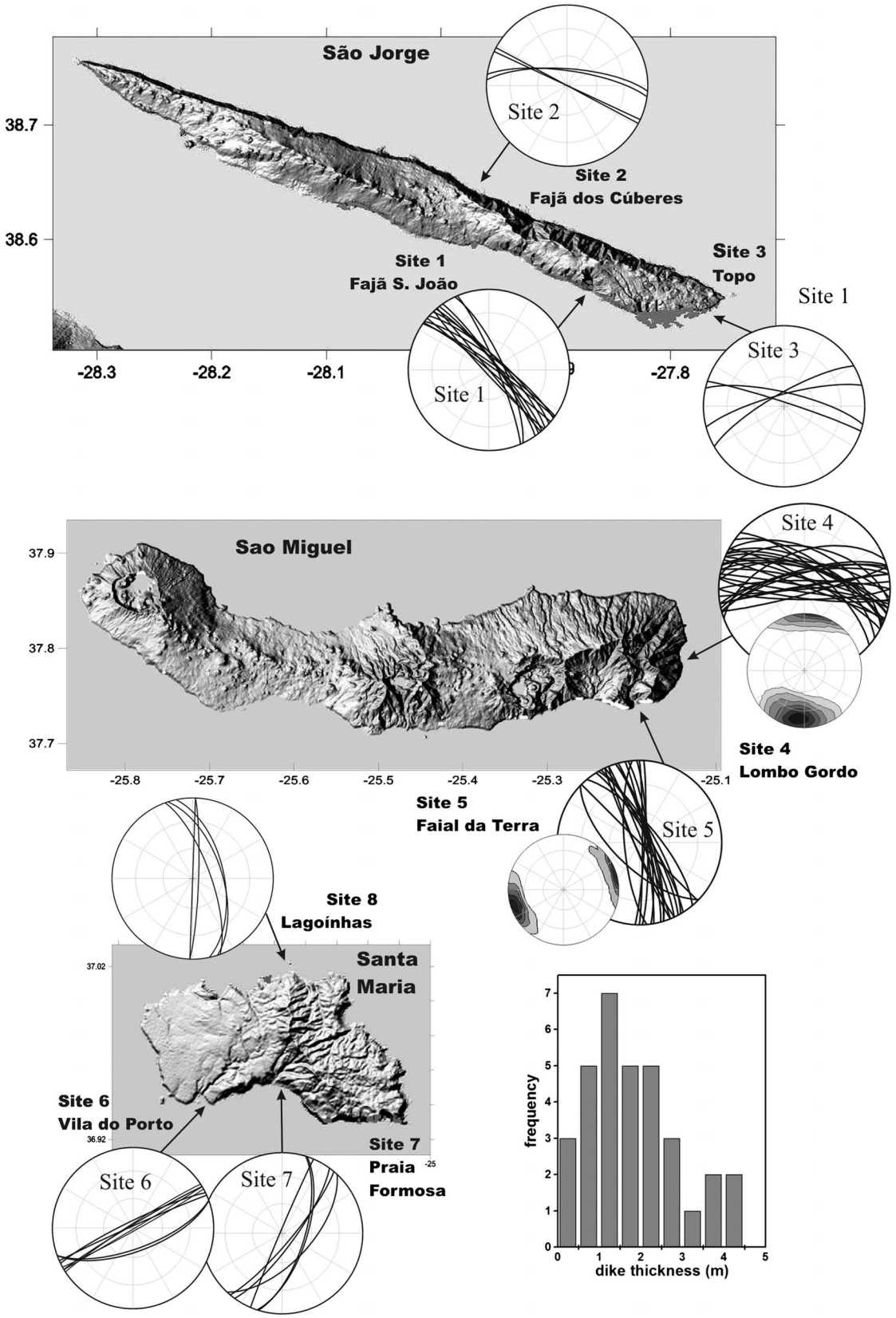

Figure 3. Location of studied sites in the islands of (top) São Jorge, (middle) São Miguel, and (bottom) Santa Maria with stereograph plots of the orientation of the sampled dyke margins. Histogram of the thickness distribution of the sampled dykes (bottom right).

©2014. American Geophysical Union. All Rights Reserved.

Table 1. Synthesis of the Localization of Sampled Sites and Number of Dykes

Island	Site	Location	Place	Coordinates	*N* Dykes	# Dykes
São Jorge	1	South	Fajã de S. João	38°34′41″N 27°55′05″W	7	1, 2, 3, 4, 5, 7, 11
São Jorge	2	North	Fajã dos Cúberes	38°38′31″N 27°58′16″W	2	8, 9
São Jorge	3	East	Ponta do Topo	38°32′32″N 27°45′39″W	2	6, 10
São Miguel	4	East	Lombo Gordo	37°47′13″N 25°08′33″W	9	1, 2, 3, 4, 5, 6, 7, 8, 9
São Miguel	5	South	Faial da Terra	37°44′35″N 25°11′11″W	3	10, 11, 12
Santa Maria	6	Southwest	Vila do Porto	36°56′44″N 25°08′43″W	4	1, 3, 4, 5
Santa Maria	7	South	Praia	36°56′57″N 25°05′26″W	4	6a, 6b, 7, 8
Santa Maria	8	North	Lagoínhas	37°00′54″N 25°05′15″W	3	9,10,11

the recent fissural volcanism, the purpose of this study is to test the hypothesis that the TRS corresponds to an accretionary axis while also elucidating the feeding mechanism of the São Jorge São Miguel and Santa Maria islands. This hypothesis would imply dominant lateral and centrifugal (radial) flows in dykes fed by the known central volcanoes. A summary of results from São Jorge has already been published [*Moreira et al.,* 1999b] and their interpretation is developed further below.

2. Geological Description

Rock samples were extracted from a total of 34 basaltic dykes, outcropping along the coast of the islands of São Jorge, São Miguel, and Santa Maria (Figure 3 and Table 1). Most of the sampled rocks show a trachytic texture. Frequently, the plagioclase microphenocrysts show strong alignment indicating a flow lineation (Figure 4).

2.1. São Jorge

São Jorge Island (Figure 3 top) belongs to the Central Group of the Azores islands. It is a WNW-ESE elongated island approximately 55 km long and a maximum width of 7 km. This linear volcano island is characterized by fissural volcanic activity that has led to the formation of approximately 200 monogenetic cones and associated *aa* lava flows.

As the other islands of the Central Group such as Faial and Pico islands, São Jorge is dominated by an active WNW-ESE tectonic direction. The alkali-basalts of São Jorge were dated earlier than 0.5 Myr [*Féraud et al*., 1980] but are now shown to be nearly 1.3 Ma [*Hildenbrand et al.,* 2008]. The island is made up of two main areas: (i) the younger western half, with numerous volcanic cones included in the two main volcanic complexes of Manadas (Pleistocene) and Rosais dated from ~0.750 Ma [*Hildenbrand et al.,* 2008], and (ii) the older eastern half of the island formed by the Topo Volcanic Complex composed mainly by the stacking of basaltic lava flows and a few dismantled cones, cut by numerous dykes [*Madeira et al.,* 1998] and dated at 1.32 Ma to 1.21 Ma [*Hildenbrand et al.,* 2008]. The main tectonic features of this island are represented by alignments of monogenetic cones along NW-SE trending eruptive fissures, WNW-ESE trending faults/volcanic rifts, and discrete normal faults. Historic volcanic activity on the island developed mainly in the Manadas Complex with two recent eruptive events recognized: Queimada in 1580 and Urzelina in 1808 [*Forjaz,* 1980; *Madeira et al.,* 1998]. Neotectonic activity along NNW-SSE to NW-SE trending normal-dextral faults is expressed by recent surface ruptures forming fault scarps [*Madeira and Brum,* 2003].

Three sites were chosen for dyke sampling all from the Topo Volcanic Complex. Site 1 at Fajã de São João located on the south shore with seven dykes sampled. Five dykes were located close to sea level and two dykes (#7 and #11) were located at 20 to 30 above sea level. The dykes trend on average NW-SE with an average dip of 80°E. Site 2 in Fajã dos Cúberes located on the north shore with two dykes sampled. Site 3

©2014. American Geophysical Union. All Rights Reserved.

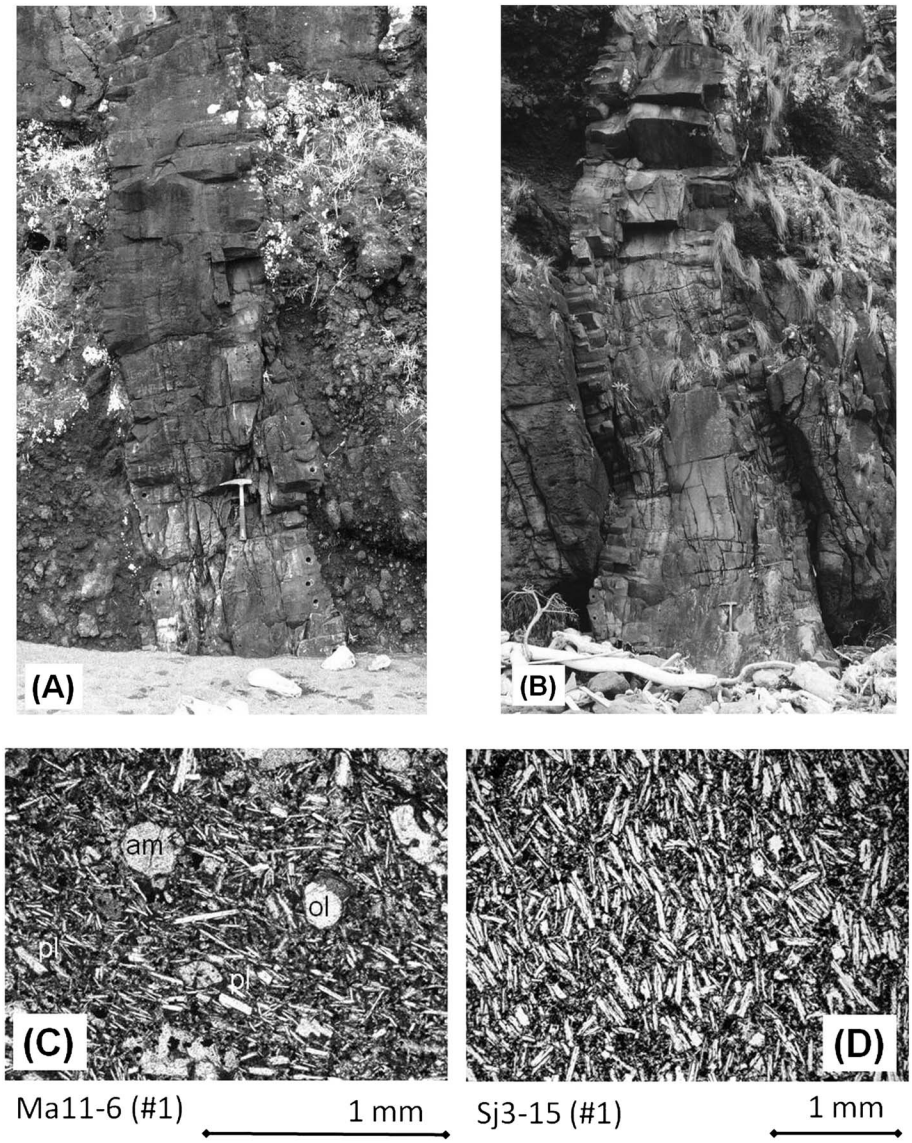

Figure 4. (top) Two typical dikes from São Miguel island—Site 1 (Lombo Gordo). (a) Dike Mi3 and (b) Mi7. Both dikes are narrow (width < 1.5 m), with well-defined margins and located around 2 m to 3 m above sea level. (bottom) Two representative microphotographies of typical rock textures and mineralogy. Trachytic texture with phenocrysts of amphibole and olivine observed in dike 11 of Santa Maria—(c) sample 6 and a typical trachytic texture with a very obvious and dense plagioclase alignment observed in dike 3 of São Jorge—(d) sample 15. Main minerals indicated are (ol) – olivine; (am) – amphibole; (pl) – plagioclase. Opaques (Fe and Ti oxides) are disseminated in ground mass.

located in Ponta do Topo the eastern extremity of the island with two dykes sampled, all at sea level. At sites 2 and 3 the dykes trend roughly E-W and are subvertical**.**

2.2. São Miguel

Located in the eastern segment of the Terceira Rift, São Miguel (Figure 3, middle) is the largest island of the Azores Archipelago. From west to east, the island is made up of four main composite active volcanoes and associated fissural systems: (1) the stratovolcano of Sete-Cidades, (2) the stratovolcano of Fogo-Água de Pau, (3) the stratovolcano of Furnas, and (4) the inactive Nordeste basaltic shield, the oldest and extensively eroded unit which includes the Povoação Caldera.

Along with the Picos Region, the Sete Cidades stratovolcano in the western part of the island is aligned NW-SE parallel with the Terceira Rift axis. In the central and eastern parts of the island, the remaining

©2014. American Geophysical Union. All Rights Reserved.

volcano-tectonic structures are offset along an E-W direction parallel to the East Azores Fracture zone. The formations are Quaternary, with the exception of the Nordeste shield, which is partly Pliocene [*Abdel-Monem et al.,* 1975; *Feraud et al.,* 1980]. Moreover, according to *Johnson et al.* [1998] using both bulk fusion and laser incremental heating techniques the alkali-basalt flow of Lombo Gordo yields a younger radiometric ^{40}Ar / ^{39}Ar age of 0.820 to 0.852 Ma. The Lombo Gordo flow yields a reverse polarity magnetization which places this formation within the Late Matuyama polarity chron. The intruding dyke swarm yields normal polarity magnetization and was likely emplaced during the Brunhes chron. The dykes belonging to this dyke swarm sampled on São Miguel were studied at two sites: Site 4 on Lombo Gordo beach, located on the east shore of the island and Site 5, located on the south coast, in the cliffs, close to Faial da Terra. The Lombo Gordo section is extensively cut by several dykes. In most of the dykes (22 out of 34 measured dykes representing 61%), the strike ranges between 075° to 105° azimuth. The dip is more variable ranging from 50°N to 80°S. From this site, 10 dykes were sampled. At Site 5, located 500 m east of Faial da Terra, the strike of 22 measured dykes ranges from 130° to 180° with subvertical dips. At this site three dykes were sampled close to sea level.

2.3. Santa Maria

The island of Santa Maria (Figure 3, bottom), in the Oriental Group, is the southeasternmost and the oldest of the Azores Archipelago. The island emerged in the Miocene (~8 Ma) [*Abdel-Monem et al.,* 1975] and the volcanic activity continued through the Pliocene. This is the only island of Azores Archipelago with marine fossiliferous sediments. It comprises two morphologically distinct domains. The western half is flat, forming a plateau with maximum elevations of 250 m above sea level. This area is composed of basaltic eruptive products from several volcanic phases as well as their associated sediments: the submarine Cabrestantes Formation, the strombolian Porto Formation, the subaerial basaltic shield comprising the Anjos Volcanic Complex, and the Touril Formation made up of marine and terrestrial sediments with minor volumes of volcanic clasts. The volcanism of the Complexo dos Anjos is essentially fissural, and the flows and dykes have an alkali-basalt composition [*Serralheiro et al.,* 1987; *Serralheiro and Madeira*, 1993]. The eastern half of the island is rugged reaching an elevation of 450 m. It is mostly built up from products of the Pliocene Facho-Pico Alto Volcanic Complex, an initially submarine volcanic ridge which progressively evolved into subaerial as the island grew eastward. The passage from submarine to subaerial volcanism in the Facho-Pico Alto Volcanic Complex is diachronic with the youngest published age for submarine lavas established at 3.2 Ma [*Feraud et al.,* 1981; *Serralheiro and Madeira*, 1993].

Dykes from Santa Maria were sampled in three localities all at sea level. Site 6 in Vila do Porto, close to the harbor (four dykes), and Site 7 at Praia Formosa (three dykes) are both located along the southern coast. These intrusions trending 050° to 070° azimuth in Site 6 and 020° to 040° azimuth at Site 7 cut the Complexo dos Anjos lava pile, but not the conglomerates and fossiliferous marine limestones of the late Miocene to early Pliocene Complexo do Touril. Site 8 (three dykes) is located in the north coast, in front of the Lagoínhas islet. The dykes show the same stratigraphic relations as observed at Sites 6 and 7 with strikes trending N-S and dipping 60°E to 75°E.

A synthesis of the localization of sampled sites and number of dykes in the three islands is presented in 1.

3. Mineral Magnetic Properties

3.1. High Field Magnetic Properties: IRM and Hysteresis

The acquisition of isothermal remanent magnetization (IRM) was studied on five specimens from four dykes on São Jorge Island. The IRM acquisition curve and the associated backfield IRM provide information on both the dominant domain state of the magnetic fraction and composition of the material. Low coercivity phases such as multidomain (MD) magnetite grains are characterized by steep acquisition with saturation at low applied fields. The measured saturation field is in most of the MD samples, between 600 and 1200 ($\times 10^{-3}$ Am^2/kg). Single-domain (SD) grains require a higher peak field to reach saturation with complete saturation around 300 mT. High coercivity phases such as hematite (Fe_2O_3), pyrrhotite (Fe_7S_8), or greigite (Fe_3S_4) do not reach saturation until well above field strength of 1.0 T fields. The results in Figure 5 show that 90% of the magnetic saturation is achieved at around 100 mT, while complete saturation is obtained at 200 mT. Backfield IRM experiments show that coercivity of remanence is achieved for fields between 10 mT and 30 mT.

©2014. American Geophysical Union. All Rights Reserved.

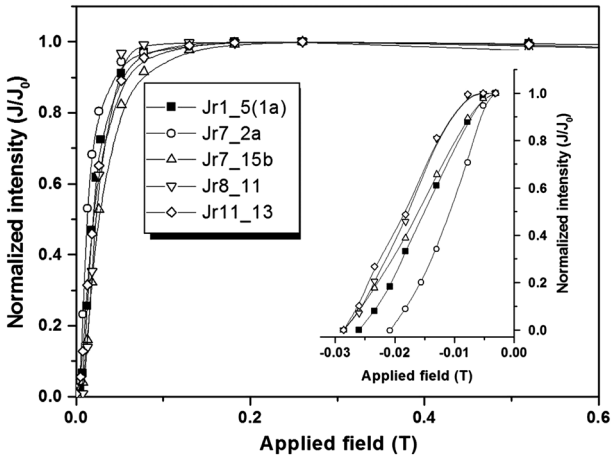

Figure 5. Representative curves of normalized isothermal remanent magnetization (IRM) acquisition and (inset) backfield IRM demagnetization for samples of São Jorge. Samples show a narrow spectrum of response with steep acquisition and reach saturation by 150 mT to 200 mT, showing no evidence of high coercivity phase. The acquisition and backfield curves are a characteristic of magnetite or titanomagnetite.

The hysteresis properties were determined for a total of 30 specimens chosen from different dykes on the three islands (25 specimens from dyke margins and five in the inner zone). The measurements were performed at the "Observatoire de Magnétisme" at the IPGP (Saint Maur, Paris) using a translation inductometer within an electromagnet. The domain state of the magnetic fraction can be determined by the ratio of hysteresis parameters H_{cr}/H_{cf}, while the relative magnetic grain size can be estimated from the magnetization ratio J_{rs}/J_s [*Day et al.,* 1977; *Dunlop and Özdemir*, 1997]. These relations are represented in a Day diagram [*Day et al.,* 1977], Figure 6 (left), while two representative hysteresis curves are shown in Figure 6 (right). The results show that the paramagnetic component is very weak. Most of the population display low coercivity ratios with $H_{cr}/H_{cf} < 2.2$, thus falling in the region of pseudo-single-domain (PSD) behavior [see *Dunlop and Özdemir*, 1997]. There is an almost linear correlation between the decrease of coercivity ratio H_{cr} / H_{cf} and the increase of the magnetization ratio J_{rs}/J_s. Nevertheless, there are specimens with high magnetization ratio that fall in the single-domain (SD) region.

Frequently, specimens with both PSD and SD magnetic state occur in the same dyke or site suggesting that mixtures of grains with different dimensions and magnetic behavior are common. High field measurements of samples from the central parts of three dykes (dykes 1 and 5 from São Miguel and dyke 4 from Santa Maria)

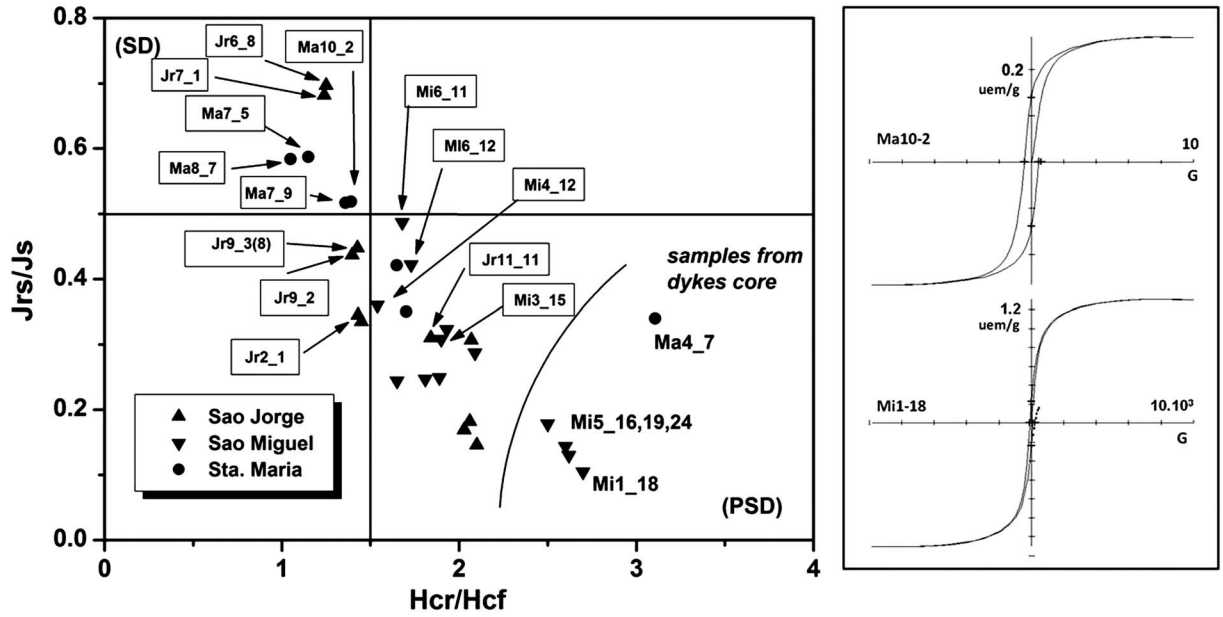

Figure 6. High field magnetic properties of selected samples from São Jorge, São Miguel, and Santa Maria. (left) Coercive field versus magnetization plotted on a Day diagram [*Day et al.* [1977]] showing the dominant pseudo-single-domain (PSD) magnetic character of most of the samples. However, samples from Santa Maria and São Jorge exhibit a single-domain magnetic character. (right) Hysteresis curves (only the ferromagnetic component) for two selected samples: Mi1-18 (PSD) and Ma10-3 (SD). Applied field H in Gauss versus magnetization J in emu/g.

©2014. American Geophysical Union. All Rights Reserved.

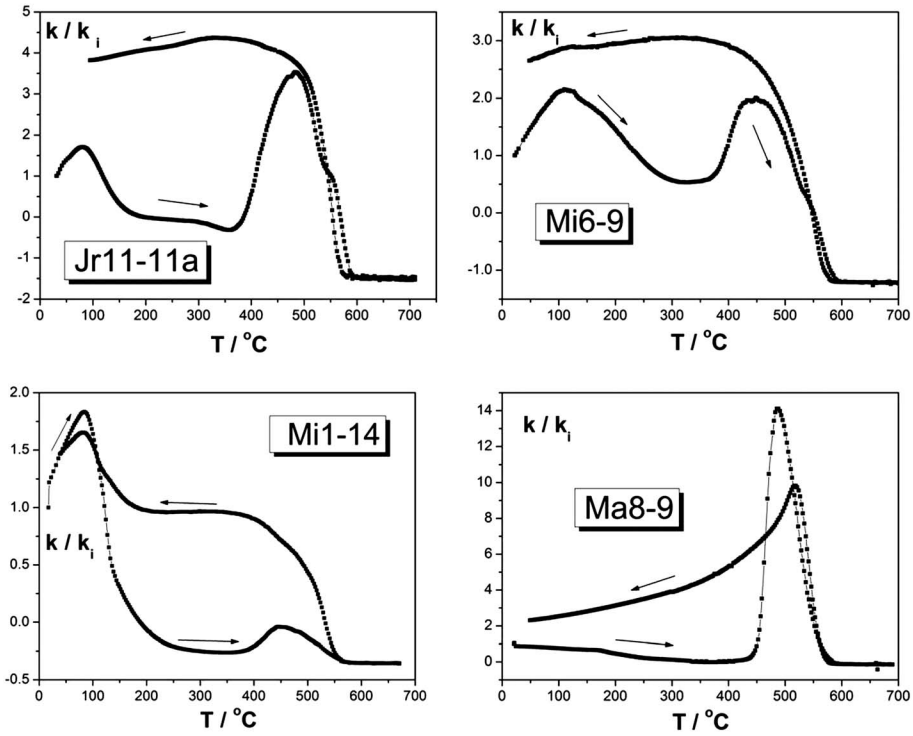

Figure 7. Representative thermomagnetic curves.

show clear differences with samples from the margins yielding higher coercivity ratios ($H_{cr}/H_{cf} > 2.5$). This result is expected since the natural slow cooling rate of the central parts of the dykes should favor larger grain size. The results indicate that the magnetic properties are mostly dominated by titanomagnetite-bearing rocks, with a prevalence of PSD character, especially in São Miguel dykes. However, there is an influence of SD particles, indicating that magnetic grains with an inverse magnetic fabric may contribute to the properties of some samples [*Rochette and Aubourg*, 1999].

3.2. Thermomagnetic Measurements

The temperature dependence of low field magnetic susceptibility, *k-T* curves, was performed on 20 samples from 15 dykes. Experiments were run in a CS2 furnace coupled to a KLY-2 Kappabridge with heating from 50°C up to a maximum of 700°C in an argon atmosphere with a steady heating and cooling rate of 9°C/min. Cycles of heating-cooling with stepwise heated curves were performed for five selected samples in a CS4 furnace coupled to an MFK1-A Kappabridge also in argon atmosphere. The Curie temperatures were estimated using the method of *Grommé et al.* [1969].

The thermomagnetic cycles show no reversibility, and in general, the occurrence of two magnetic phases (e.g., Jr11-11a and Mi6-9 in Figure 7). There is a variation of behavior of the curves according to the relative importance of the low- and high-temperature magnetic phase.

The low-T_C magnetic phase yields Curie temperatures in a relatively large range of $200° < T_C < 350°C$. With further heating, the susceptibility increases steeply until a very sharp decrease is again observed, defining a second magnetic phase. The obtained Curie temperatures T_C of this second phase lies between 560° and 590°C. In some samples this high-T_C phase yields high values of susceptibility (e.g., Ma8-9 in Figure 7), while in other samples the increase in the susceptibility is much lower (e.g., Mi1-14, Figure 7).

The cooling curve shows usually higher susceptibility values than the heating curve and does not reproduce the heating behavior, especially in the high temperatures range. Approaching low temperatures ~ 200°–250°C the cooling curve tends to approach the shape of the heating curve. The final magnetic susceptibility at room temperature, at the end of the cooling phase, is usually higher than the initial magnetic susceptibility (Figure 7).

©2014. American Geophysical Union. All Rights Reserved.

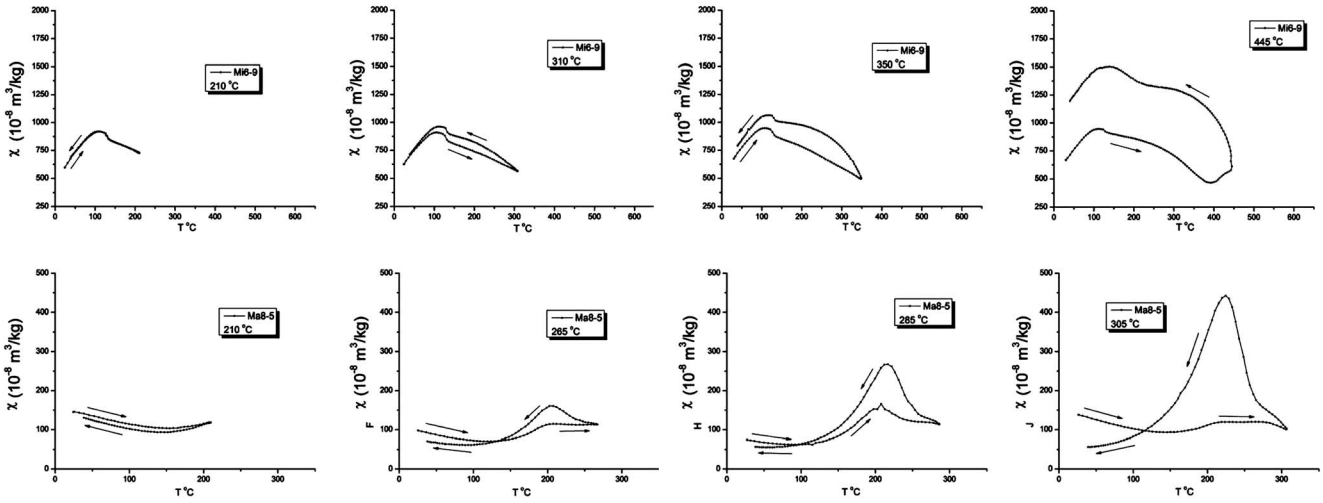

Figure 8. Representative cycles of heating-cooling with stepwise heated curves of two samples. Up to ~ 200°–225°C, the process is reversible. But for higher temperatures a new magnetic phase begins to develop.

Cycles of heating-cooling with stepwise heated curves show (Figure 8) that the *k-T* curves are practically reversible for cycles reaching 200°–225°C revealing again the low-T_C magnetic phase. After a heat phase up to 300°C the cooling curve begins to diverge from the corresponding heating curve. From a temperature of 300°C and higher the behavior of the heating and cooling susceptibility curves is clearly different, showing the formation and growth of a magnetic phase with high T_C. The T_C of this new phase falls in the range 560°–590°C indicating the formation of magnetite which is in agreement with the fact that in the end of the cycles the final magnetic susceptibility at room temperature is usually higher than the initial susceptibility.

The progressive increase of the susceptibility that occurs around 300°–400°C that is not observable in the cooling curve indicates the formation in the heating process of a magnetic phase, most probably of a titanomaghemite solid solution. The formation of that phase at 250°–300°C with a Curie temperature around 560°–590°C is indicative of magnetite formed during heating by the inversion of the maghemite [*Dunlop and Özdemir*, 1997].

Concluding, these results define a magnetic composition characteristic of a solid solution of Ti-rich titanomagnetite with large range of percentages of titanomaghemite. As a result of the heating above 250°–300°C mineral alterations begin to occur. The temperature where these transformations occur and the obtained magnetic mineral is compatible with the process of transformation of titanomaghemite, which is metastable, being converted through a process of inversion. The new magnetic phase is a solid solution with a composition between titanomagnetite and magnetite, including as well other minor phases such as ilmenite or hematite [*Özdemir*, 1987; *Dunlop and Özdemir*, 1997].

The observed range of T_C of the low-temperature phase reveals a solid solution of titanomagnetite Ti-rich with different degrees of low-temperature oxidation. The variation of the relative susceptibility of the secondary magnetic phase, due to mineral alteration induced by temperature, is an indicator of the occurrence of different percentages of the titanomaghemite slightly oxidized.

3.3. Chemical Analyses

To supplement the study of the magnetic properties of the matrix and microcrystalline oxide phases, chemical analyses were conducted on six specimens from dykes of Santa Maria and São Miguel using an Electron Probe Microanalyzer JEOL-JCXA 733 at the Geologic Department of the Faculty of Sciences of the University of Lisbon. Data are summarized in Tables 2 and 3.

The dominant minerals include plagioclase (≈ 20% to 26% in Santa Maria samples and ≈ 40% in São Miguel samples), pyroxene (≈13% to 23% in Santa Maria samples, < 10% in São Miguel samples), and Fe-Ti oxides (usually ≈ 10% to 15%, with the exception of one sample from Santa Maria with a low content of ≈ 3%).

©2014. American Geophysical Union. All Rights Reserved.

Table 2. Main Composition of the Sampled Basalts of Santa Maria and São Miguel Dykes

		Santa Maria-Praia			São Miguel-Lombo Gordo		
		Ma7-12b	Ma7-6	Ma8-6	Mi1_14	Mi3_10	Ml6_8
Microphenocrystal component (%)	Plagioclase	8.4	8.4	23.3	11.9	5.1	0.2
	Amphibole	1.7	5.1		2.2	0.6	
	Oxides	0.4			1.0	5.3	
	Piroxene					1.1	
	Olivine						
Matrix component (%)	Plagioclase	20.6	24.0	26.0	40.5	37.5	37.5
	Piroxene	3.1	22.8	13.5	5.0	7.5	9.5
	Oxides		12.4	14.6	10.5	12.6	13.1
Fine matrix component (%)		64.8	26.6	21.3	15.0	18.8	23.7
Vesicles (%)		1.1	0.4	1.1	13.7	10.6	15.5

The oxides are normally distributed into two groups: Ti-rich spinels, sometimes occurring in the skeletal form, and ilmenites. Magnetite is scarce. Only sample Ma8-6 displays a distinctive composition with micrometric grains of magnetite with a calculated chemical formula of $Fe^{3+}_{1.98}\ Fe^{2+}_{1.04}\ O_4$ and a large percentage of plagioclases (49.3%) and oxides (14.6%).

The composition of the oxides plotted on the ternary diagram of Figure 9 is defined by the chemical formula $Ti_x\ Fe_{(3-x)}\ O_4$, with $x = 0.65 \pm 0.12$. These values indicate that the oxide phase contained in the basalts corresponds to a titanomagnetite solid solution, mainly Ti-rich in composition which is in agreement with the conclusions from the thermomagnetic measurements. Nevertheless, there exists a large spectrum of variation in the compositions. The deviations from the theoretical line of the titanomagnetite solid solution and the departure of the ilmenites composition from the theoretical FeTiO reflect an oxidation process or maghemitization (low-temperature oxidation of the titanomagnetite). Despite the mainly Ti-rich composition of the solid solution, chemical analysis shows that "pure" magnetite grains are present in samples. This

Table 3. Chemical Composition of the Spinels[a]

	Santa Maria-Praia				São Miguel-Lombo Gordo				
	Ma7_12		Ma7_6	Ma8_6	Mi1_14		Mi3_10		Mi6_8
%	*C*	*M*	*M*	*M*	*C*	*M*	*C*	*M*	*M*
Al_2O_3	5.23	5.27	5.23	3.54	5.53	2.20	5.14	2.62	3.86
MgO	4.74	2.75	4.31	1.28	6.03	1.81	5.39	1.09	2.75
MnO	0.48	0.68	0.53	0.67	0.29	0.65	0.29	0.51	0.41
V_2O_3	1.15	1.49	0.79	1.22	1.13	1.39	0.76	0.82	1.49
TiO_2	20.54	25.77	21.15	29.84	16.76	21.32	17.46	18.85	19.30
ZnO	0.00	0.02	0.00	0.03	0.00	0.02	0.00	0.02	0.04
NiO	0.03	0.00	0.00	0.00	0.08	0.01	0.11	0.01	0.04
FeO	64.13	55.64	63.97	54.44	64.98	67.16	65.94	70.81	67.63
Cr_2O_3	0.05	0.02	0.05	0.09	1.00	0.02	0.93	0.10	0.00
Total	96.03	91.63	96.10	91.12	95.80	94.58	96.02	94.83	95.52
Al	1.78	1.91	1.80	1.32	1.86	0.79	1.73	0.94	1.35
Mg	1.89	1.26	1.86	0.62	2.56	0.82	2.30	0.49	1.21
Mn	0.13	0.18	0.13	0.18	0.07	0.17	0.07	0.13	0.10
V	0.31	0.37	0.18	0.31	0.26	0.34	0.17	0.20	0.35
Ti	4.57	5.84	4.59	7.12	3.59	4.87	3.75	4.30	4.29
Zn	0.00	0.01	0.00	0.01	0.00	0.00	0.00	0.00	0.01
Ni	0.01	0.00	0.00	0.00	0.02	0.01	0.03	0.00	0.01
Fe^{2+}	10.62	12.55	10.69	14.33	9.06	11.93	9.47	11.17	11.06
Fe^{3+}	4.72	1.77	4.76	0.11	6.41	5.28	6.30	6.17	5.66
Cr	0.00	0.00	0.01	0.02	0.22	0.01	0.21	0.02	0.00
O	32.00	32.00	32.00	32.00	32.00	32.00	32.00	32.00	32.00

[a]Chemical composition of the spinels in sampled basalts of Santa Maria and São Miguel dykes. *C*: percentage in the crystal; *M*: the percentage in the matrix.

©2014. American Geophysical Union. All Rights Reserved.

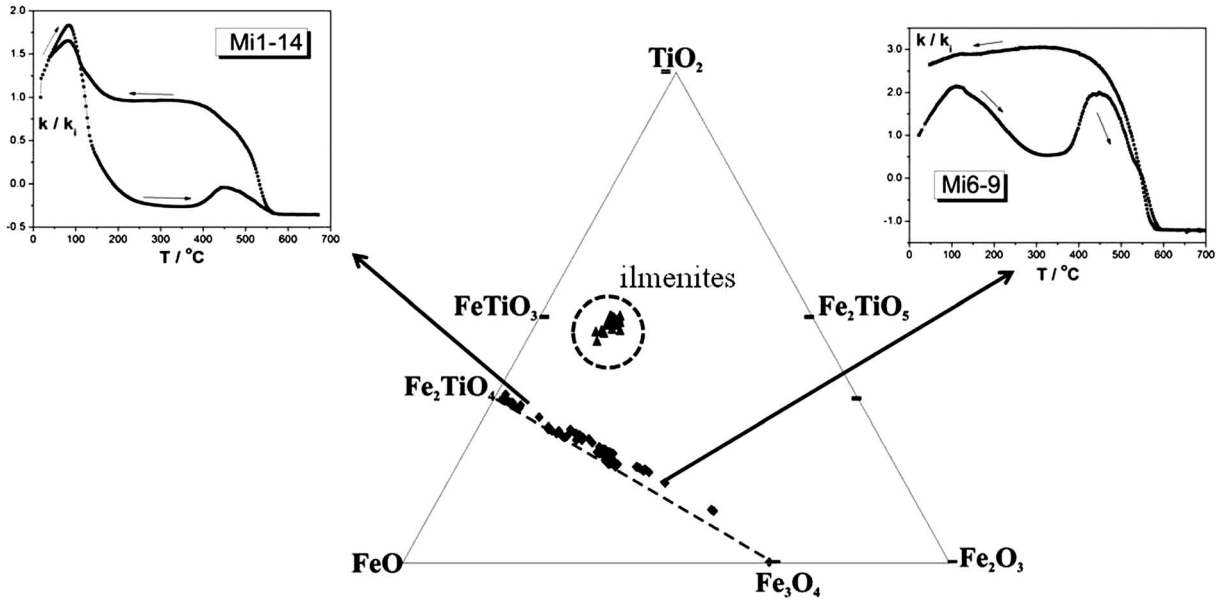

Figure 9. Compositional analysis plotted on a ternary diagram with two representative thermomagnetic analyses. This plot shows the range of the composition of the titanomagnetite solid solution and the slight departure from the theoretical titanomagnetite series toward higher *O* contents. The ilmenites plot, away from the theoretical composition, revealing an oxidation effect.

resultagrees with the high field measurements which indicate a SD character for some samples of São Jorge and Santa Maria.

In conclusion, the results indicate a large range of composition of the titanomagnetites Ti-rich, slightly oxidized with different percentages of the titanomaghemite.

4. AMS Sampling and Results

4.1. Magnetic Susceptibility and Anisotropy

The origin and geophysical applications of the anisotropy of magnetic susceptibility are extensively explained in several text books and specialized articles [e.g., *Tarling and Hrouda*, 1993; *Rochette et al.,* 1992; *Butler,* 1992; *Tauxe et al.,* 2012].

In an isotropic medium, the magnetic volume susceptibility k is a scalar parameter defined by the ratio between the induced magnetization J and the applied magnetic field H, according to the expression: $J = k/H$. If the medium is anisotropic the above relation can be rewritten as $J_i = k_{ij}H_j$ $(i, j = 1, 2, 3)$, where J_i is the magnetization in the direction i and H_j the applied magnetic field in the direction j. As J and H are expressed in Am^{-1} (SI), the volume susceptibility k is dimensionless. The coefficients of the magnetic susceptibility k_{ij} are the elements of a second-order symmetric tensor called Anisotropy of Magnetic Susceptibility (AMS).

For a weak-inducing field (the induction bridges Kappabridge KLY-2 and KLY-3 use 300 Am^{-1}, at 920 Hz and 875 Hz, respectively [*Hrouda*, 2002]) the magnetization is linear and reversible which means that k_{ij} is also symmetric. The diagonal and symmetric terms of this tensor measure the induced magnetization in three orthogonal directions. These three diagonal terms with magnitudes $k_1 \geq k_2 \geq k_3$ are the maximum, intermediate, and minimum susceptibility axes of the anisotropy of magnetic susceptibility ellipsoid. The mean susceptibility k_m is determined by $(k_1 + k_2 + k_3)/3$. The AMS is conventionally represented as a triaxial ellipsoid whose major, intermediate, and minor axes correspond to the respective directions and magnitudes of the magnetic susceptibility. If $k_1 = k_2 = k_3$, the ellipsoid is spherical. When $k_1 \approx k_2 > k_3$, the ellipsoid is oblate (flattened or disk shaped), and when $k_1 > k_2 \approx k_3$, the ellipsoid is prolate (acute or needle shaped).

The AMS ellipsoid may be characterized by several parameters among which the most used being the directional parameters, i.e., the magnetic lineation L, defined as the direction of the k_1 axis and the magnetic foliation F, defined by the plane containing the k_1 and k_2 axes, which is perpendicular to the k_3 axis.

©2014. American Geophysical Union. All Rights Reserved.

Anisotropy is quantified by the corrected degree of anisotropy P' where

$P' = \exp\sqrt{2\left((\ln(k_1/k_m))^2 + (\ln(k_2/k_m))^2 + (\ln(k_3/k_m))^2\right)}$ and also by the magnetic lineation $L = k_1/k_2$, the magnetic foliation $F = k_2/k_3$ and the shape of the AMS ellipsoid (or shape parameter) defined as $T = (2(\ln k_2 - \ln k_3)/(\ln k_1 - \ln k_3)) - 1$. The shape parameter T may be visualized on a k/T diagram where the oblate shapes fall in the positive T region ($0 \leq T \leq 1$) and prolate shapes in the negative T region ($-1 \leq T \leq 0$). The definitions of many other shape parameters are given in *Jelinek* [1981], *Tarling and Hrouda* [1993], *Hrouda* [1982], *Borradaile* [1988], and *Rochette et al.* [1992].

In mafic igneous rocks, the minerals responsible by the magnetic fabric are the Fe-Ti oxide solid solutions, titanomagnetites and titanohematites. The main contributions to the AMS at the microscopic scale are due to (1) the anisotropic shape of grains or shape anisotropy and (2) the crystallographic anisotropy of the grains or magnetocrystalline anisotropy [e.g., *Graham*, 1954; *Stacey,* 1960; *Elwood*, 1978; *Rochette et al.,* 1992]. Furthermore, in ferromagnetic igneous rocks (e.g., basalts) where titanomagnetite is the main contributor to the magnetic signal, the observed anisotropy is a result of both the intrinsic anisotropy or grain shape of magnetite (the magnetocrystalline anisotropy is very weak as the mineral has a cubic crystal structure) and of the distribution of magnetic particles between the silicate phases [*Hargraves and Johnson,* 1991].

4.2. Sampling

The sampled dykes have a mean thickness of 1.8 ± 1.4 m (Figures 3, 4a, and 4b). The sampling was carried out along the chilled margins of the dyke, usually no more than 10 cm from the contact with the host rock. Dykes were not sampled if they showed weathered margins, ambiguous or imprecise contact with the country rock, or if they exhibited closely spaced columnar joints. The orientations of cored samples and local dyke margins were measured with a magnetic compass. To check the local variations of magnetic declination or abnormal dyke remanence, solar determinations of strike azimuth were carried out at each site. We sampled a total of 34 dykes on the three islands, representing 66 sampled margins. From this set, we obtained a total of 413 core samples, from which 559 cylindrical specimens were cut with the usual dimensions of 2.5 cm diameter and 2.2 cm long.

4.3. Magnetic Susceptibility and Shape Parameters

The specimens were measured to obtain the principal axes k_1 (maximum), k_2 (intermediate), and k_3 (minimum), using low alternating inductive field bridges KLY-2 and KLY-3 Kappabridge. The magnitude and orientation of the magnetic ellipsoid of each specimen was calculated using the *Jelinek* [1978] statistics, and the mean directions and confidence zones were calculated using the statistical method of *Henry and Le Goff* [1995].

To systematize the directional information of the AMS at the scale of the dyke, the AMS of the specimens for each margin was plotted according to a common reference, related to the average orientation of that margin. Because the margins may show local undulations which significantly change the local strike and dip values, we measured the orientation of the margins in the vicinity of each sampled point. Then by rotating the magnetic axis of each sample to a common direction defined by two axes (i.e., the strike and dip directions), we are able to integrate the AMS axes of all samples with respect to a common reference frame. In this way the orientation of the magnetic anisotropy axes of each sample is related to a common plane corresponding to the mean strike and dip orientation of the margin. The mean directions and confidence limits of the AMS of each margin are then calculated using all the specimens of that margin based on the statistical method of *Henry and Le Goff* [1995]. Tables 4–6 report the results obtained for the following AMS parameters: mean magnetic susceptibility (k), the corrected degree of anisotropy (P'), shape parameter (T), magnetic lineation (L), and foliation (F).

The magnetic susceptibility of the dykes ranges from $k = 2.0 \times 10^{-3}$ to 50×10^{-3} International System of Units (SI), with a mean susceptibility $k = 16.3 \pm 11.8 \times 10^{-3}$ SI units (Figure 10). The dykes of São Jorge island yield a magnetic susceptibility k usually lower than 35×10^{-3} SI—analogous to the results obtained by *Silva et al.* [2012]—while the values obtained for Santa Maria are lower than $k = 25 \times 10^{-3}$ SI. In the case of São Miguel, the dykes show not only a wider range of magnetic susceptibility but also higher values in the range $k = 35 \times 10^{-3}$ to 45×10^{-3} SI.

©2014. American Geophysical Union. All Rights Reserved.

Table 4. AMS Results for São Jorge Dykes[a]

Site	Dyke Margin	Margin Orientation	N	k	k_1	e_{12}	e_{13}	k_3	e_{31}	e_{32}	Fab	L	F	P'	T
1	Jr1/NE	145/82°E	6	6.4	320/41	11	23	51/8	7	19	N	1.009	1.013	1.041	0.181
1	Jr1/SW	155/75°E	6	7.4	19/73	6	27	236/24	5	18	N	1.017	1.017	1.038	0.000
1	Jr2/NE	157/82°E	5	11.9	138/76	3	28	243/3	2	5	N	1.012	1.033	1.052	0.463
1	Jr2/SW	157/82°E	7	20.1	250/81	20	21	133/35	6	24	I	1.016	1.019	1.069	0.085
1	Jr3/NE	130/90	7	25.1	347/71	1	2	229/10	1	8	N	1.045	1.010	1.062	−0.631
1	Jr3/SW	132/76°E	8	27.6	85/53	5	30	219/29	4	7	N	1.004	1.019	1.031	0.650
1	Jr4/NE	127/78°E	7	14.7	53/69	10	27	252/30	15	24	N	1.015	1.002	1.031	−0.763
1	Jr4/SW	142/82°E	8	14.3	3/76	7	11	212/15	11	19	N	1.030	1.012	1.052	−0.425
1	Jr5/NE	156/77°E	11	9.8	97/53	5	13	213/29	9	21	N	1.026	1.002	1.037	−0.856
1	Jr5/SW	139/81°E	11	12.6	178/63	3	11	71/4	3	14	N	1.054	1.020	1.083	−0.453
1	Jr7/NE	125/83°E	14	17.9	148/47	8	25	29/24	6	10	N	1.002	1.011	1.021	0.691
1	Jr7/SW	140/90	10	25.8	133/9	3	9	229/37	3	6	N	1.007	1.021	1.030	0.497
1	Jr11/NE	126/86°E	9	7.9	147/64	7	16	32/6	5	10	N	1.012	1.010	1.028	−0.090
1	Jr11/SW	317/86°W	8	7.8	136/57	2	7	32/9	4	8	N	1.031	1.008	1.044	−0.586
2	Jr8/N	115/90	11	23.1	315/13	7	19	49/3	3	10	N	1.007	1.038	1.054	0.685
2	Jr8/S	118/90	14	22.4	142/55	13	27	232/5	3	13	N	1.003	1.024	1.038	0.776
2	Jr9/N	098/75°N	6	6.9	50/51	12	38	193/47	11	23	N	1.008	1.005	1.018	−0.230
2	Jr9/S	094/73°N	7	6.3	297/42	7	24	182/20	8	17	N	1.009	1.004	1.017	−0.384
3	Jr6/N	075/78°N	7	3.7	322/77	10	19	181/10	5	11	N	1.011	1.017	1.033	0.213
3	Jr6/S	060/77°N	11	5.4	35/67	5	24	127/1	3	14	N	1.009	1.049	1.072	0.684
3	Jr10/N	103/76°N	12	18.6	285/53	2	16	189/9	1	6	N	1.004	1.017	1.026	0.617
3	Jr10/S	108/86°N	10	9.4	192/70	7	21	32/15	5	18	N	1.004	1.023	1.033	0.701

[a]AMS results after tensorial analysis for São Jorge dykes. For each dyke both margins are indicated with the respective azimuth and inclination relative to the horizontal, in the direction indicated N: number of specimens measured; k: mean magnetic susceptibility in 10^{-3} SI units; k_1: direction and azimuth of k_1 axis; e_{12} and e_{13}: half confidence angles at 95% for k_1 axis; k_3: direction and azimuth of k_3 axis; e_{31} and e_{32}: half confidence angles at 95% for k_3 axis, angles in degrees; Fab: magnetic fabric. N = normal, I = inverse, A = other; L, F, P', and T: respectively lineation, foliation, corrected degree of anisotropy, and shape parameter.

Table 5. AMS Results for São Miguel Dykes[a]

Site	Dyke Margin	Margin Orientation	N	k	k_1 D/I	e_{12}	e_{13}	k_3 D/I	e_{31}	e_{32}	Fab	L	F	P'	T
4	Mi1/N	081/51°N	5	42.9	25/64	9	23	199/24	9	19	N	1.021	1.028	1.050	0.141
4	Mi1/S	090/81°N	5	35.7	267/63	10	20	168/2	7	13	N	1.009	1.019	1.026	0.355
4	Mi2/N	081/79°N	11	21.1	286/51	5	18	184/7	5	8	N	1.017	1.020	1.038	0.080
4	Mi2/S	083/86°S	11	23.6	119/69	29	8	346/15	4	12	N	1.020	1.016	1.037	−0.110
4	Mi3/N	095/82°N	11	20.4	136/57	13	21	8/28	8	18	N	1.010	1.015	1.025	0.199
4	Mi3/S	104/66°N	9	18.5	32/60	5	19	178/28	5	8	N	1.022	1.018	1.040	−0.099
4	Mi4/N	061/71°N	7	13.8	140/55	4	33	259/13	4	7	I	1.009	1.014	1.023	0.216
4	Mi4/S	063/84°N	8	13.6	135/60	5	24	253/11	5	9	I	1.008	1.013	1.022	0.237
4	Mi5/N	092/59°N	8	12.6	343/56	4	11	199/27	5	6	N	1.016	1.012	1.028	−0.142
4	Mi5/S	085/65°N	5	16.8	40/76	8	32	257/29	13	27	I	1.014	1.013	1.029	−0.037
4	Mi6/N	081/59°N	5	10.5	21/67	7	9	217/19	7	46	A	1.029	1.009	1.011	−0.523
4	Mi6/S	082/62°N	6	20.1	30/69	6	6	291/5	5	39	A	1.004	1.007	1.038	0.272
4	Mi7/N	115/80°N	13	21.7	13/50	10	21	275/26	12	20	I	1.012	1.009	1.022	−0.142
4	Mi7/S	096/85°N	14	28.1	181/16	17	9	1/61	26	11	A	1.016	1.014	1.031	−0.066
4	Mi8a/N	094/79°N	11	42.7	312/62	8	12	203/10	8	11	N	1.013	1.017	1.031	0.132
4	Mi8a/S	104/86°N	10	44.4	312/66	13	23	194/9	9	12	N	1.012	1.021	1.034	0.271
4	Mi8b/N	086/69°N	4	21.8	87/18	5	31	183/18	2	7	N	1.007	1.020	1.028	0.479
4	Mi8b/S	088/77°N	9	25.6	65/13	10	23	161/20	6	11	N	1.009	1.019	1.028	0.355
4	Mi9/N	079/79°N	6	22.5	12/71	7	20	184/9	11	15	N	1.024	1.019	1.044	−0.115
4	Mi9/S	096/84°S	5	20.1	86/22	13	40	357/8	17	25	N	1.014	1.020	1.035	0.175
5	Mi10/E	159/86°E	5	20.6	298/77	3	12	119/16	2	24	A	1.038	1.017	1.059	−0.377
5	Mi10/W	125/68°W	7	19.1	245/68	10	17	40/18	6	16	N	1.019	1.030	1.047	0.222
5	Mi11/E	155/75°E	4	16.4	214/84	6	16	114/5	4	23	A	1.030	1.028	1.059	−0.034
5	Mi11/W	135/74°E	8	12.7	138/58	5	15	357/21	7	17	I	1.021	1.009	1.032	−0.398
5	Mi12/E	151/81°E	7	8.3	169/84	2	9	247/2	8	12	N	1.048	1.031	1.082	−0.211
5	Mi12/W	147/87°E	7	7.7	119/80	3	8	245/6	2	13	N	1.029	1.035	1.065	0.092

[a]AMS results after tensorial analysis for São Jorge dykes. For each dyke both margins are indicated with the respective azimuth and inclination relative to the horizontal, in the direction indicated N: number of specimens measured; k: mean magnetic susceptibility in 10^{-3} SI units; k_1: direction and azimuth of k_1 axis; e_{12} and e_{13}: half confidence angles at 95% for k_1 axis; k_3: direction and azimuth of k_3 axis; e_{31} and e_{32}: half confidence angles at 95% for k_3 axis, angles in degrees; Fab: magnetic fabric. N = normal, I = inverse, A = other; L, F, P', and T: respectively lineation, foliation, corrected degree of anisotropy, and shape parameter.

©2014. American Geophysical Union. All Rights Reserved.

Table 6. AMS Results for Santa Maria Dykes[a]

Site	Dyke Margin	Margin Orientation	*N*	*k*	k_1 *D/I*	e_{12}	e_{13}	k_3 *D/I*	e_{31}	e_{32}	Fab	*L*	*F*	*P′*	*T*
6	Ma1/N	066;88°N	11	17.3	324;76	12	27	186;7	6	10	*N*	1.009	1.016	1.027	0.278
6	Ma1/S	070;66°S	5	17.4	96;45	15	43	321;21	10	13	*N*	1.011	1.018	1.029	0.240
6	Ma3/N	059;89°S	5	10.4	267;55	13	37	166;2	9	12	*N*	1.012	1.016	1.027	0.142
6	Ma3/S	070;69°S	7	15.6	95;21	17	25	351;17	7	21	*N*	1.027	1.072	1.093	0.446
6	Ma4/N	057;86°N	6	14.0	32;81	7	12	135;2	4	10	*N*	1.016	1.030	1.049	0.301
6	Ma4/S	061;87°S	7	17.1	59;77	7	26	330;1	7	10	*N*	1.009	1.020	1.031	0.377
6	Ma5/N	059;87°N	5	16.0	191;72	11	21	305;3	8	18	*N*	1.003	1.007	1.011	0.399
6	Ma5/S	064;83°N	4	15.2	241;47	17	22	158;1	18	24	*N*	1.005	1.003	1.009	−0.250
7	Ma6a/W	017;67°E	9	71.3	51;60	8	27	278;24	4	13	*N*	1.004	1.011	1.015	0.465
7	Ma6b/E	017;67°E	8	2.2	139;81	14	26	265;15	16	20	*N*	1.005	1.004	1.009	−0.111
7	Ma6b/W	012; 70°E	5	2.6	128;29	18	25	290;37	16	45	*N*	1.003	1.003	1.013	0.000
7	Ma7/SE	036;77°E	8	2.8	112;62	9	19	333;19	6	16	*N*	1.010	1.009	1.019	−0.052
7	Ma7/W	033;88°W	4	2.9	124;73	10	19	277;10	13	22	*N*	1.006	1.006	1.012	0.000
7	Ma8/SE	040;80°SE	3	3.7	92;2	3	10	189;63	5	7	*I*	1.004	1.006	1.010	0.200
7	Ma8/NW	043;61°E	6	3.5	90;19	13	29	205;69	11	21	*I*	1.003	1.014	1.019	0.645
8	Ma9/E	162;60°E	4	6.5	139;37	5	10	239;14	4	6	*N*	1.008	1.019	1.029	0.405
8	Ma9/W	182;84°E	4	6.3	171;35	8	47	280;25	3	12	*N*	1.013	1.022	1.036	0.255
8	Ma10/E	168;58°E	8	6.1	92;17	7	39	226;57	4	18	*N*	1.033	1.081	1.128	0.412
8	Ma10/W	160;72°E	5	8.1	14;66	5	32	256;18	3	9	*N*	1.049	1.057	1.123	0.074
8	Ma11/E	182;90	8	3.4	345;76	25	34	157;22	10	22	*I*	1.010	1.006	1.016	−0.249

[a]AMS results after tensorial analysis for São Jorge dykes. For each dyke both margins are indicated with the respective azimuth and inclination relative to the horizontal, in the direction indicated *N*: number of specimens measured; *k*: mean magnetic susceptibility in 10^{-3} SI units; k_1: direction and azimuth of k_1 axis; e_{12} and e_{13}: half confidence angles at 95% for k_1 axis; k_3: direction and azimuth of k_3 axis; e_{31} and e_{32}: half confidence angles at 95% for k_3 axis, angles in degrees; Fab: magnetic fabric. *N* = normal, *I* = inverse, *A* = other; *L*, *F*, *P′*, and *T*: respectively lineation, foliation, corrected degree of anisotropy, and shape parameter.

The average corrected degree of anisotropy in the studied dykes is low, with $P' = 1.039 \pm 0.028$. Nevertheless, some specimens may reach values as high as $P' = 1.115$ in dyke 3 or $P' = 1.187$ in dyke 10, both from Santa Maria. The *P′*-*T* diagram (degree of anisotropy versus shape parameter in Figure 11) show that, on average, the specimens from São Jorge yield both oblate- and prolate-shaped ellipsoids, whereas for São Miguel and Santa Maria, oblate shapes are predominant. However, some exceptions exist, such as dykes from Site 1 of São Jorge and dykes from Site 5 on São Miguel, where most of the margins show specimens with a dominance of lineation.

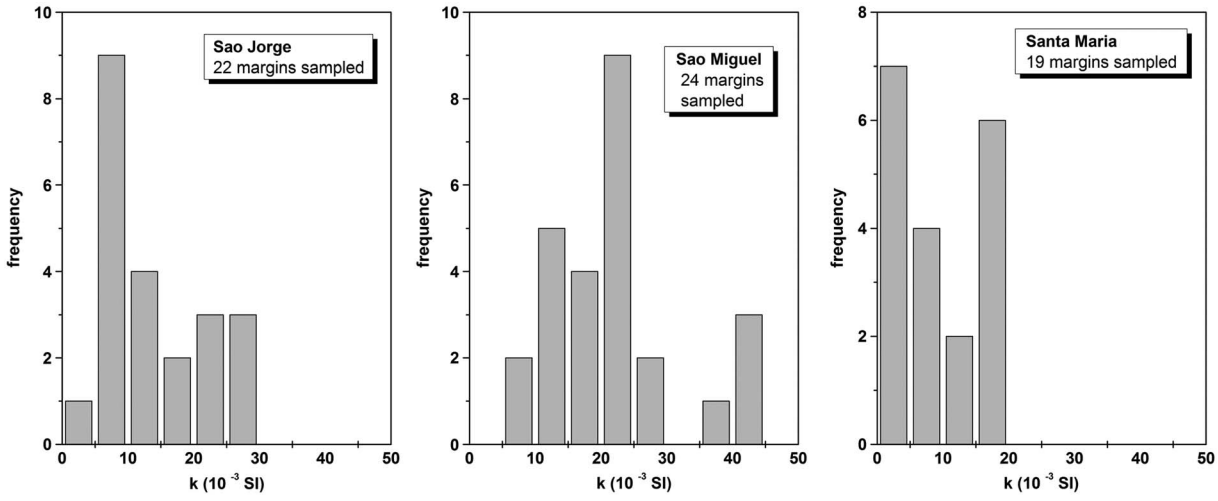

Figure 10. Histograms for the magnetic susceptibility of the dykes (average over each margin) from São Jorge, São Miguel, and Santa Maria. With the exception of two dykes from São Miguel, the magnetic susceptibility is always below 30×10^{-3} SI.

©2014. American Geophysical Union. All Rights Reserved.

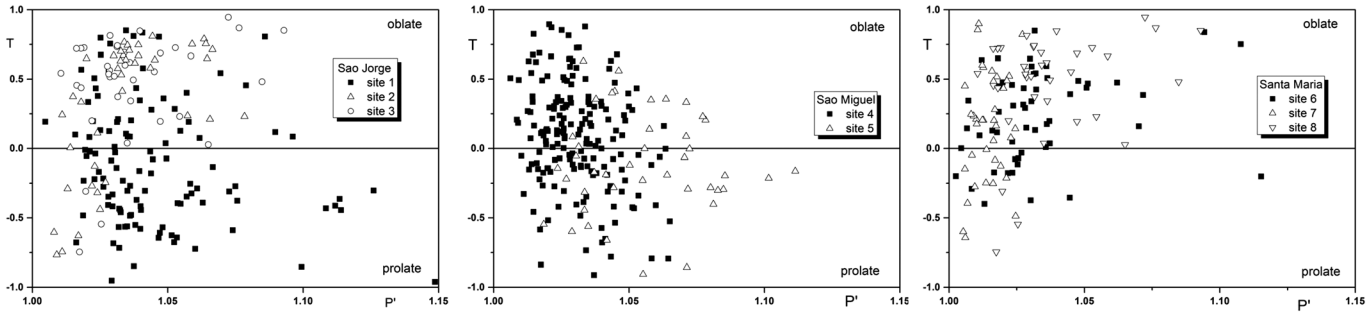

Figure 11. The *P'-T* relationship for dykes of São Jorge, São Miguel, and Santa Maria.

4.4. Magnetic Fabric: Shape and Orientation

The AMS data were plotted on equal area (lower hemisphere) stereographic projections with AMS axes k_1 (squares), k_2 (triangles), and k_3 (circles). Filled symbols represent the mean tensor with the associated confidence ellipses.

At the scale of the dyke "normal fabrics," according to the definition of *Rochette et al.* [1991], are largely dominant. In 52 out of 66 (~78%) of the sampled margins, labeled in Tables 4–6 by *N* (normal), the magnetic fabric shows that the k_3 axis close to the normal of the dyke and the magnetic foliation plane is subparallel to the dyke margin (e.g., Figures 12a and 12b). Moreover, in most of the dykes with normal fabrics at both margins, the imbrication angle between of the magnetic foliation plane (MFP) and the margin is broadly symmetrical relatively to the dyke axis. The measured MFP-dyke wall angles range between 10° and 30° in 37 margins (56%) with a mean value of 18°.

Out of the remaining 14 margins, nine margins (i.e., ~14%) yield a magnetic foliation plane that is roughly perpendicular to the dyke plane (Figure 12c), with the k_3 axis close to the plane of the dyke, indicating an inverse magnetic fabric (Mi3, Mi4, Mi5-south margin, Jr9-north margin) and labeled as *I*. These dykes yield a shape of ellipsoid similar to the normal fabric dykes, but their magnetic susceptibility is usually lower than the average value measured in the normal fabric dykes. For example, the Lombo Gordo dykes with an inverse magnetic fabric (Mi4, Mi5-south, or Mi7 north) yield $k = 17.5 \times 10^{-3}$ SI ($\pm 3.3 \times 10^{-3}$ SI), while the dykes with normal fabric show $k = 28.4 \times 10^{-3}$ SI ($\pm 10.5 \times 10^{-3}$ SI). The remaining five margins (i.e., ~8%) yield an abnormal magnetic fabric labeled here as *A*, which is characterized by a more dispersed clustering of axes or with the mean k_3 parallel or very close to the margin orientation (Figure 12d).

The dispersion of the magnetic lineation k_1 is greater than the k_3 axis. Therefore, the mean magnetic foliation plane is more constrained than the magnetic lineation. In 43 of the 66 of sampled margins (representing 65%), the average radius of confidence of k_3 mean direction is less than 10°. In fact, the k_3 axis clusters are tightly constrained with 95% confidence ellipses of ($e_{23} = 11.1 \pm 5.9$) having smaller areas than for the k_1 axis clusters ($e_{12} = 15.3 \pm 7.7$).

5. Magma Flow Vectors Estimated by AMS

5.1. The Use of AMS to Infer Fossilized Magma Flow Vectors in Dykes

The magmatic flow fabric in a dyke is represented by the fabric of the early crystallized phenocrysts, usually with high aspect ratios that act as rigid particles. The mechanism that promotes the preferred orientation of phenocrystals in a conduit, assuming a Newtonian laminar flow, is due to the mechanical drag and force moment produced close to the interface between the magma and the solid wall. In the vicinity of a dyke's wall, the flow induces a strain gradient regime characterized by simple shear that changes to pure shear in the central part of the dyke. According to *Ildefonse et al.* [1992] or *Arbaret et al.* [1996], even low concentrations of phenocrysts particles should interact and become aligned with their long axes at a low angle to the flow direction. This spatial arrangement is expressed by a tiling pattern which determines an imbrication angle for the phenocrysts relative to the margin where the shear gradient is higher.

©2014. American Geophysical Union. All Rights Reserved.

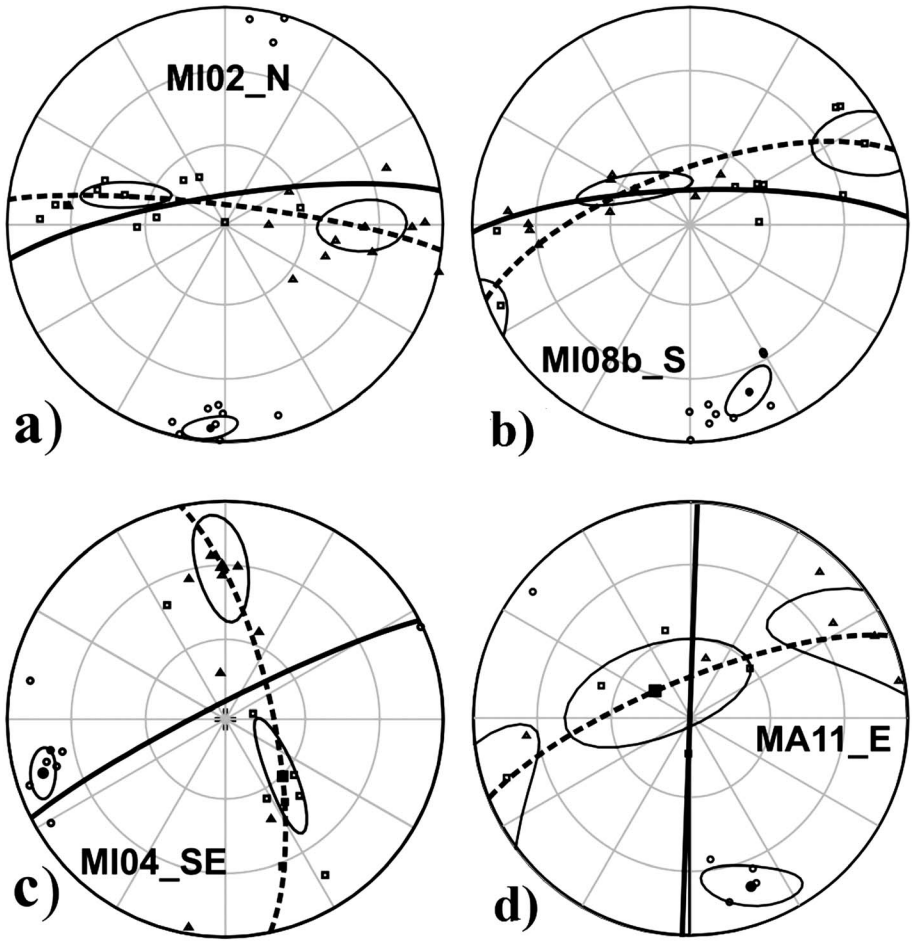

Figure 12. Representative magnetic fabrics for dykes plotted in geographic coordinates on equal area stereographic projections (lower hemisphere). AMS principal axes are k_1 (squares), k_2 (triangles), and k_3 (circles). Filled symbols are the mean tensor within ellipses of statistical confidence. Projection of dyke margin (thick continuous line) and magnetic foliation plane, MFP (dotted line). (a and b) Two examples of normal magnetic fabric in dyke 2, north margin and dyke 8b south margin, from Site 4, São Miguel. (c) One example of an inverse magnetic fabric obtained from the southeast margin of dyke 4 in São Miguel. (d) A high dispersion magnetic fabric from the east margin of dyke 11, Site 8 in Santa Maria.

The imbrication of the phenocrysts provides information on the sense of shear and, in some cases, the shape of the strain ellipsoid can be connected to the fabric. In a simple model without along-plane displacement of the walls, the imbrication would be symmetric relative to the dyke axis producing a theoretical symmetrical fabric [*Knight and Walker*, 1988]. In such cases, the magnetic fabric is linked to the preferred orientation (shape or alignment) of magnetic minerals that are developed between the phenocrystals, and thus becomes a proxy of the magmatic flow fabric.

Such a relationship between the magmatic flow and the AMS in dykes was proposed by *Knight and Walker* [1988], based on the relation between orientation of magnetic axes and orientation of the elongated vesicles at the margins of the dykes. They concluded that the orientations of k_1 axes and the observed imbrication angle between k_1 axes at each margin could be interpreted to determine the orientation of the flow vector.

However, in some circumstances, the magnetic lineation may not be directly related to the flow direction. *Jeffery* [1922] demonstrated that noninteracting prolate rigid particles immersed in a fluid with laminar flow are aligned with the long axis normal to both the velocity of flow and the direction of its maximum gradient. For high shear strains, particles should interact and tend to align their long axes at low angle to the flow

©2014. American Geophysical Union. All Rights Reserved.

direction. Both *Khan* [1962] and *Elwood* [1978] pointed out that, in dykes, k_2 could also be aligned with the flow line. *Elwood* [1978, p. 263] stated that "In dykes, emplacement direction is represented by either an azimuth normal to a non-random k_a (i.e. k_1) axial mean or by a direction parallel with the azimuth of a non-random k_b (i.e. k_2) mean,"

Magnetic lineations perpendicular to the flow direction were also subsequently reported by *Knight and Walker* [1988], *Dragoni et al.* [1997], and *Philpotts and Philpotts* [2007].

The size of magnetic grains also affects the magnetic fabric behavior. Indeed, in magnetite-bearing rocks, multidomain magnetite shows a normal magnetic anisotropy, meaning that the maximum susceptibility is oriented parallel to the long axis of the grain, while single-domain magnetite (broadly with grain lengths $< 0.1\ \mu m$) yields an inverse magnetic fabric, where the easy axis of magnetization is perpendicular to the long axis of the grain [*Tarling and Hrouda*, 1993; *Potter and Stephenson*, 1988; *Ferré*, 2002; *Chadima et al*., 2009]. Thus, mixtures of different grain sizes or strong interaction between ferromagnetic grains [*Hargraves and Johnson,* 1991; *Canon-Tapia*, 1996; *Gaillot et al.,* 2006] may imply an intermediate magnetic fabric [*Rochette and Aubourg*, 1999] which can complicate the interpretation. Ambiguities that may arise from an interpretation based on the magnetic lineation were also pointed out by *Aubourg et al.* [2002, 2008] and *Geoffroy et al.* [2002, 2007]. Using a comparison between the AMS axes and preferred orientation of plagioclases in oriented thin sections of mafic dykes from the East Greenland volcanic margin led *Geoffroy et al.* [2002] to show that the angular deviation between the magnetic lineation and plagioclases orientation display a bimodal distribution, meaning that either k_1 or k_2 is parallel or close to the alignment of phenocrysts. As pointed out by *Callot and Guichet* [2003], another ambiguity stems from the possible combination of highly planar or composite rock textures, very common in magmatic rocks, which may lead to an apparent magnetic lineation, or "zone axis" due to the intersection direction of different magnetic foliation planes. A new problem arises also when a composite fabric is developed during dyke emplacement in which the ferrimagnetic and paramagnetic fabrics may not be coaxial. *Silva et al.* [2014] analyzed this problem in the doleritic dyke Foum Zguid. They concluded that is most probably the paramagnetic fabric that is associated with the magma flow direction, while the ferrimagnetic and AMS (which yield similar fabrics) are associated to late-stage cooling stress and as a consequence not directly related to the flow fabric. Despite the fact that these results were obtained from a thick dyke, the different behaviors of individual fabrics in a composite fabric rock justify all the prudence in the interpretation of the relationship of the AMS axis with the magmatic flow direction.

As a consequence, it is incorrect to assume as a rule that the magnetic principal axis k_1 represents the flow direction everywhere along a dyke; this hypothesis is not corroborated and detailed rock experiments must be performed to establish the magnetic mineral grain size as well the magnetic and the mineral flow fabrics relationship.

5.2. Petrofabric Analysis of Preferred Orientations of Mineral Phases

We performed a petrofabric analysis to asses the uncertainty discussed above concerning the interpretation of the magnetic lineation as the preferred orientation of the longer axis of opaque ferromagnetic grains, (broadly the whole set of Fe and Ti oxide minerals) and its relation to the orientation of phenocrysts (mainly plagioclases). Our aim was to quantify the angular difference between the directions of the principal magnetic axes, obtained from the AMS measurements, and to correlate these results with the alignment of phenocrystals and opaques in 2-D space as observed on microscopic images.

Forty thin sections cut parallel to the magnetic foliation plane were prepared from 25 cores representing 18 different dykes using the cylindrical specimens selected for the AMS study. From each thin section several high-resolution images were digitized. After image filtering to separate phenocrysts (mainly plagioclases) from opaque phases, we used the "Intercept" software to obtain the statistical directional distribution of the minerals. This algorithm creates a rose (or polar distribution) of mean intercept lengths that is calculated for the intersection of boundaries of a phase or mineral selected in the image and constructed with a Fourier decomposition up to a chosen harmonic. The obtained rose of directions show usually a long axis (first harmonic) a short axis (second harmonic), and, depending of the Fourier analysis degree, some minor orientations more or less scattered [*Launeau and Robin*, 1996].

©2014. American Geophysical Union. All Rights Reserved.

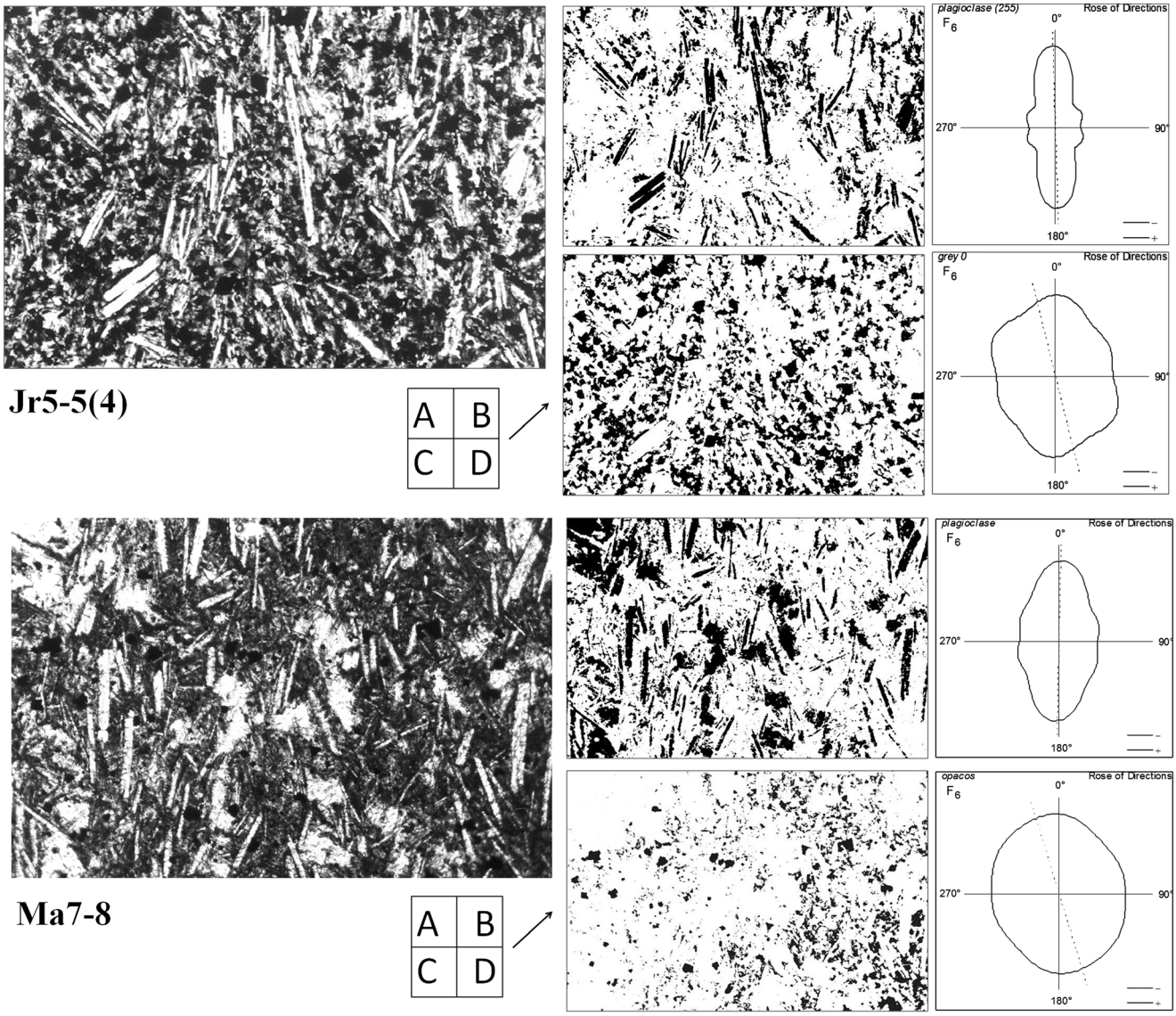

Figure 13. Two examples of the microtextural analysis of plagioclases and opaques preferred orientation based on thin section microphotographs, using the Intercept method [*Launeau and Robin*, 1996]. This algorithm is based on the analyses of boundaries of objects, called phases, which may represent a type of individual mineral, discontinuity, border, or texture. The counting of the intercepts by Fourier series produces a rose of intercepts from which we can derive a directional rose diagram (alignments or preferred orientations). Results are obtained numerically and graphically in the form of roses diagrams, showing the directions and mean shape of minerals. The directional roses of the mineral boundaries of selected phase indicate the preferred elongation axis or orientation of the considered phase. This procedure was applied for the study of phenocrysts—mainly plagioclases—and opaque grains in a total of 49 microphotographs from 40 thin sections cut from 25 cores extracted from 18 different dykes. Two representative examples from samples Jr5-5(4) and Ma7-8, with the original image on the left. (a) The processed image used to analyze the plagioclases (inverted color); (b) the obtained directional rose diagrams; (c) the processed image used to analyze the opaques, and (d) the obtained directional rose diagrams.

We used the direction of the long axis of the rose of directions, as the maximum of the preferred orientation, here designated as maxPO to study the correlation with the orientation of the k_1 magnetic axis in the plane of the image, parallel with the foliation plane (Figure 13).

The angular deviation between the maxPO of ferromagnetic opaques and phenocrystals (Figure 14a) shows a monomodal distribution. In most of the observations (75%), the angle between the maxPO of the two minerals is less than 20°. We may infer that in the magnetic foliation plane k_1-k_2, the preferred orientations of opaques and phenocrysts are mostly coaxial.

©2014. American Geophysical Union. All Rights Reserved.

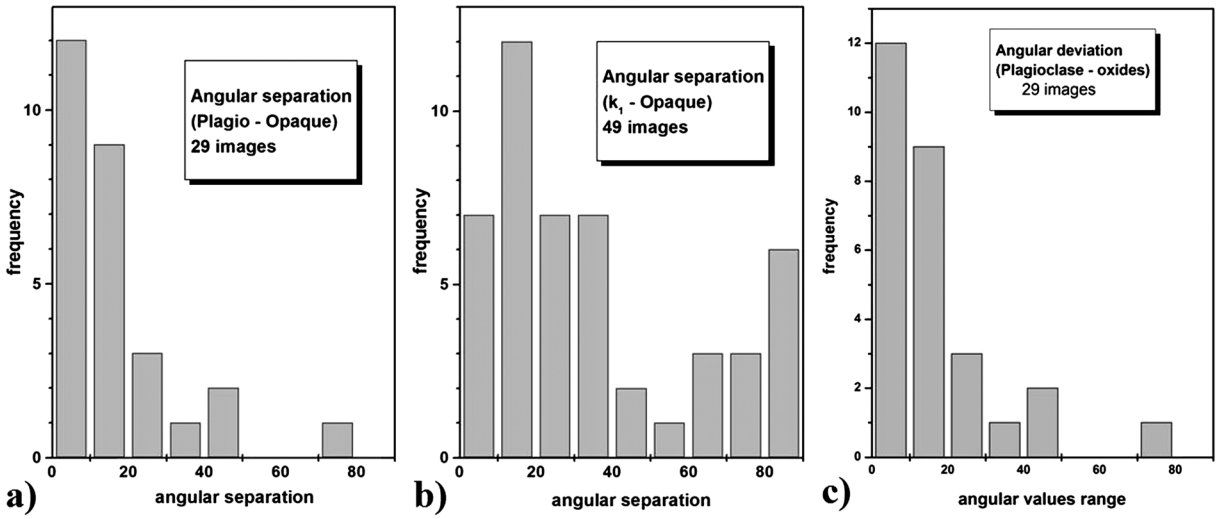

Figure 14. Diagrams showing relationship between the maxPO of opaques and phenocrysts as a function of the orientation of the magnetic lineation k_1. Histograms of (a) the angular separation between maxPO of phenocrysts and opaques, (b) k_1 and maxPO of opaques, and (c) k_1 and maxPO of phenocrysts.

However, an analysis of the relationship between maxPO of opaques and k_1 direction yields a bimodal distribution (Figure 14b). At first order the angular differences are around 20° with second-order differences approaching 80° to 90° which is close to the k_2 axis. The difference between the orientation of the opaques and the k_1 axis is less than 30° in 51% of the studied cases, but it is greater than 60° in 24% of the thins sections, meaning that the maxPO of the opaques tends here to be close to the orientation of the k_2 axis.

It is interesting to note that the specimens which show a maxPO of opaque grains closer to the k_2 axis (Ma3-21, Ma4-4, Ma7-8, Jr4-8(1), Jr5-4, and Jr10-11b) display a normal rather than an inverse magnetic fabric. This behavior is observed in prolate and oblate specimens, with high or low anisotropy; so it seems not to be dependent of the shape of the ellipsoid of susceptibility or anisotropy. Besides, the k_2 axis is systematically with low inclination. With the exception of the specimen Mi5-1b that presents an inverse magnetic fabric, this low inclination is coincident with the inclination of the deduced magmatic flow vector of that particular margin.

The remaining 15% of images relating maxPO of opaques and k_1 directions shows intermediate angular separations, ranging between 30° and 60°.

The angular differences between the magnetic lineation and the maxPO of the phenocrysts are presented in Figure 14c. While these data also yield a slight bimodal correlation, it is here superposed on an almost continuous range of values of different angular separations ranging from 0° (coaxial) to 90° (perpendicular).

From these results, we conclude that (1) within the foliation plane the maxPO of oxide grains (opaques) is essentially coaxial with the orientation of the phenocrysts and (2) the maxPO of both opaques and plagioclases is split into two orthogonal directions: one direction being coaxial with the magnetic lineation and other perpendicular.

The angular relationships obtained between maxPO of minerals (opaques and phenocrysts) and the magnetic lineation axis show that, on average, either k_1 or k_2 may be coaxial with the preferred orientation of the dominant phase, i.e., plagioclase, thus giving rise to an ambiguity in the directional relationship.

5.3. Magmatic Flow Direction Inferred by AMS Measurement

As previously discussed (section 4.4), the orientation of the k_3 axis is more constrained than the k_1 axis. At the scale of the dykes margin, confidence angles are smaller around k_3 axes than around k_1 axes. Moreover, in the dykes with a normal magnetic fabric the magnetic foliation planes define imbrications angles which open symmetrically with respect to the dyke axis, thus defining a unique magma flow direction (Figures 12a, 12b,

©2014. American Geophysical Union. All Rights Reserved.

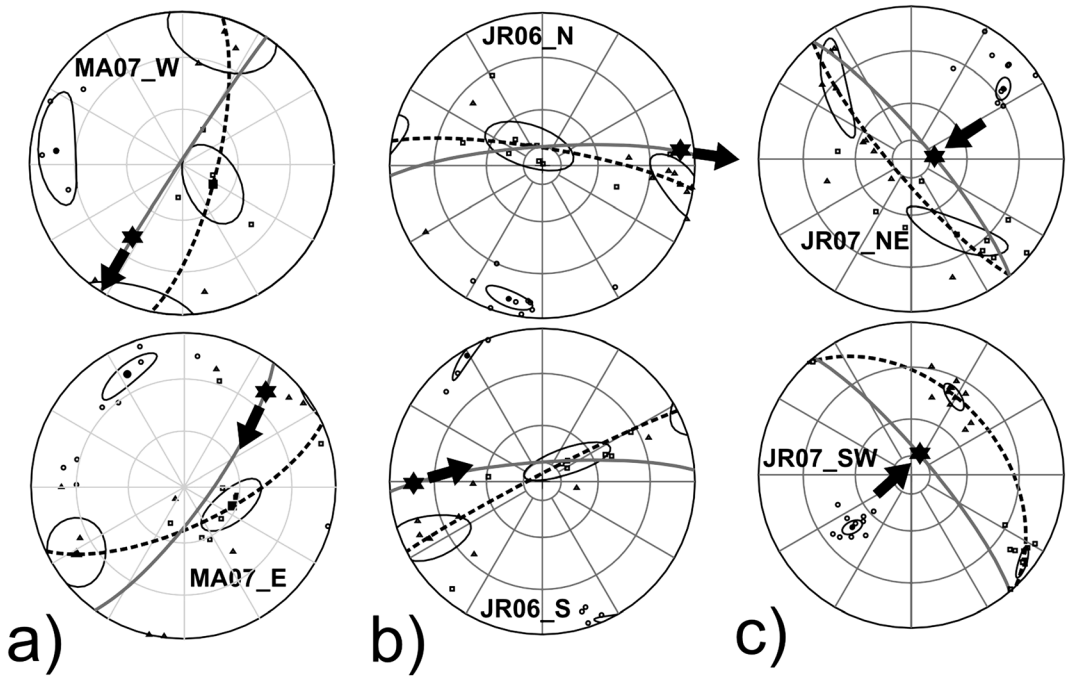

Figure 15. Representative examples of flow vector determinations for three dykes according to the explanations in text. Legend of the stereonet was explained in Figure 12. Solid arrow represents the direction and sense of the inferred flow vector. (a) Dyke 7 of Santa Maria, northwest margin (top) and southeast margins (bottom). The imbrication angles are 25° and 29°, respectively. Flow vector points (direction/inclination) 212°/40° (down) in northwest margin and 41°/20° (up) in southeast margin. The sense of the flow is coherent in both margins, i.e., southwest with low inclination. (b) Dyke 6 of São Jorge, margins north (top) and south (bottom). The imbrication angles are 15° and 24°, respectively. Flow vector points (direction/inclination) 83°/8° (down) in north margin and 89°/19° (up) in south margin. The sense of the flow is coherent at both margins, i.e., east and subhorizontal. (c) Dyke 7 of São Jorge, northeast (top) and southwest (bottom) margins. The imbrication angles are of 20° and 38°, respectively. Flow vector points (direction/inclination) 45°/80° (down) in the northeast margin and 69°/79° (down) in the south margin. The sense of the flow is coherent at both margins, almost vertical and downward. This flow sense is probably associated with a "subsidence" of the magma in the dyke during the final phases of intrusion and not related to the geometry of flow during the intrusion.

and 15). In 44 out of the 66 sampled margins (≈ 67%), the magnetic foliation planes strike at angles between 10° and 30° relative to the respective margins.

The interpretation of the image analysis (section 5.2) shows that there is no simple relationship between the magnetic lineation, the PO of phenocrysts, and the assemblage of magnetic mineral phases. To avoid the uncertainty in choosing arbitrarily the k_1 or k_2 axis to describe the flow trend and given the small but overall dominant oblate fabrics (Figure 11), the flow vector would be best determined using the "attitude" of the magnetic foliation plane relative to the margin dyke. To define a unique flow direction, we consider the imbrication of the magnetic foliation plane relative to the dyke margin, following the model explained in detail by *Geoffroy et al.* [2002] (Figure 2) and *Geoffroy et al.* [2007] (Figure 6), to define unique flow direction. This proposed method makes use of the imbrication angle of the magnetic foliation plane relative to the margin plane as an indicator of the magmatic flow direction and sense. Assuming, as previously mentioned, a Newtonian rheology and no displacement at the margins of the dyke in the final phases of the intrusion flow, the magnetic fabric at the dyke margin can be used to determine the flow vector geometrically, for each dyke margin. This can be performed on each dyke wall using the perpendicular to the axis of intersection between the magnetic foliation plane and the dyke wall plane. The sense of the flow vector is obtained by considering the orientation of the imbrication angle between the magnetic foliation and the dyke wall.

Representative examples of this analysis are shown in Figure 15 for dyke 7 from Santa Maria and dykes 6 and 7 from São Jorge. In each case, both margins yield concordant results concerning the sense of the flow, predominantly horizontal in the first two dykes and dominantly vertical in the last one.

©2014. American Geophysical Union. All Rights Reserved.

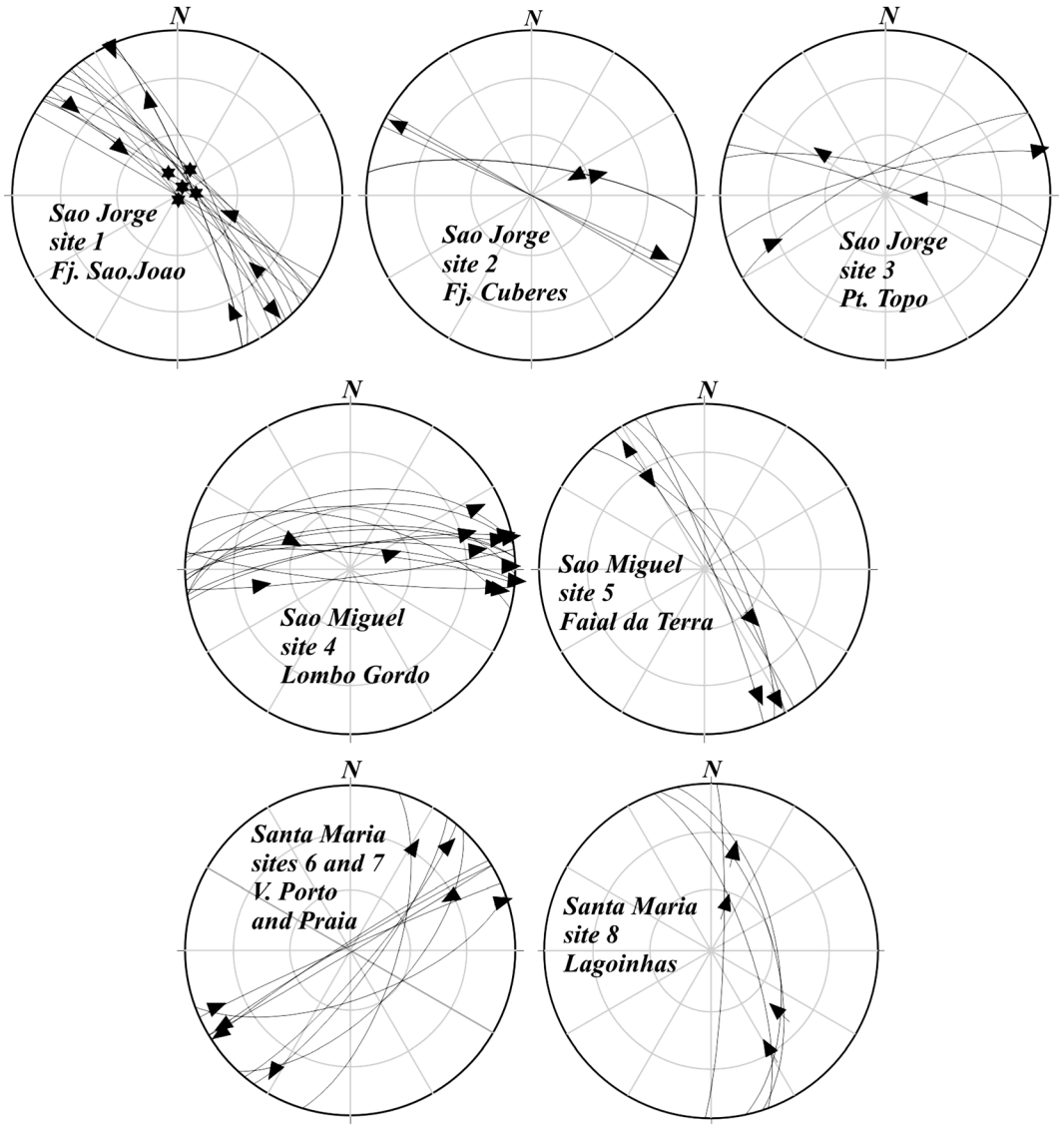

Figure 16. Inferred flow vectors represented by arrows for all dyke margins. Solid stars for Site 1 on São Jorge represent the inferred flow vectors of high plunge values observed in dyke 7 (both margins) and in one of the margins of dykes 1, 3, and 11. The dyke margins are represented in their geographic orientations in equal-area stereographic projections (lower hemisphere).

5.4. Flow Vectors in the Azores Dykes

In the case of 19 dykes it was possible to obtain interpretable data from both margins. However, for five of these dykes we obtain opposite flow vectors from each margin. To obtain an overview of the whole data set, we plot in Figure 16 the flow vectors for all of the 48 interpretable margins observed at each of the studied sites.

For the São Jorge dykes, we obtain 21 margins with normal magnetic fabric. For 10 of these margins, the flow vector has an inclination of less than 40°, while nine margins show an inclination greater than 45°. In the remaining two margins, the principal magnetic axes are scattered. These dykes show a complex flow pattern due to the coexistence of low inclination and subvertical flow vectors. Interestingly, the vertical flow vector in dyke Jr7 (see Figure15c) yields a "downward" sense of the flow. This is probably an effect of flow convection within the dyke related to the final stages of magma emplacement and subsequent reflux and/or deflation of magma into the dyke. This result is not uncommon and has been reported at different sites

©2014. American Geophysical Union. All Rights Reserved.

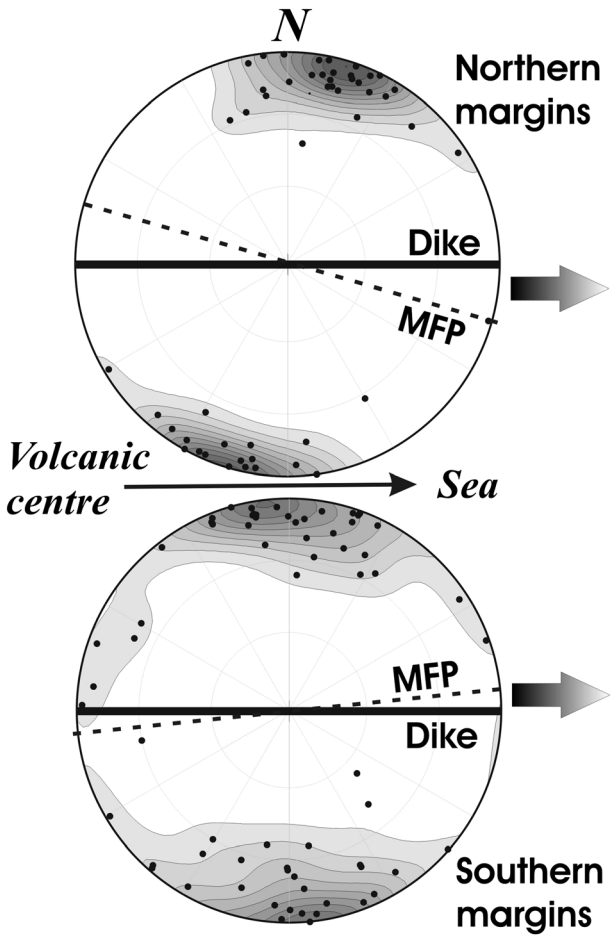

Figure 17. Contour levels of k_3 vectors from the transformed margins of dykes from the Site 4 Lombo Gordo on São Miguel. All margins and their respective magnetic fabrics were rotated to a common reference frame, defined as a vertical E-W oriented dyke allowing an overall visualization.

(e.g., East Greenland dykes [*Callot and Geoffroy,* 2004], including rhyolitic dykes from Ponza island [*Aubourg et al.,* 2002], in a tholeitic dyke swarm of the Isle of Skye [*Geoffroy et al.,* 2007], in a camptonite dyke of the Higby Mountain in New England [*Philpotts and Philpotts*, 2007], in dykes on Tenerife [*Soriano et al.,* 2008], or at the scoria cone of Lemptégy [*Petronis et al.,* 2013]).

On São Miguel, the flow vectors obtained at both sampled sites are very consistent, indicating a predominantly horizontal or low inclination flow with a sense from west to east (in 10 out of 13 margins with a normal magnetic fabric) at Lombo Gordo Site 4 (east shore) and broadly from northwest to southeast (in four of five margins with normal magnetic fabric) at the Faial da Terra Site 5, located on the south shore (Figure 16). To highlight the fact that the majority of the inferred flow vectors from these two sites imply a flow away from a common central source, we grouped all the data together by rotating all margins and their associated fabrics according to a common reference frame. This reference frame corresponds to a synthetic dyke with an arbitrary E-W strike and a vertical dip that is close to the average attitude of the dykes from Site 4. Figure 17 shows the density contours of the k_3 axes along with the mean magnetic foliation plane and the (synthetic) dyke. This representation outlines the coherent imbrications angles indicating an unambiguous direction and sense of the magmatic flow, which is thus lateral and centrifugal apart from the Nordeste basaltic shield.

On Santa Maria Island, the obtained flow vectors are also predominantly horizontal at Sites 6 and 7 with a predominant north-to-south sense (Vila do Porto and Praia sites, south shore of the island) and oblique flow with a systematic south-to-north sense of flow at Site 8 (Lagoínhas, on the northern shore). This is noteworthy because all the dikes from these sites are contemporaneous. The orientation of the dykes from these three sites defines a converging point, located close to the apex of Pliocene Pico Alto Volcanic Complex. Since these dykes are older than this volcanic center, they are probably not associated with the subsequent Pico Alto magmatic events but rather to a former magmatic center located near the same position. The existence of such magmatic structure is consistent with an important magnetic anomaly of reverse polarity—Figure 6 in *Storetvedt et al.* [1989]—which is broadly centered on this zone. Our data and interpretations indicate a steeper inclination of the magmatic flow in dykes from Site 8 (Lagoínhas at north) and a predominant horizontal to subhorizontal magmatic flow from Sites 6 and 7 (in the south). This is in agreement with the presence of a shallow magmatic center located in the central northern part of the island, with a centrifugal propagation of dykes away from this center. Dykes sampled on the north shore are closer to the magmatic center, which implies a steeper magmatic flow, while dykes on the south shore show predominantly lateral or subhorizontal flow geometry.

©2014. American Geophysical Union. All Rights Reserved.

Table 7. Imbrication Angles and AMS Parameters for Site 4[a]

Samples From	Mean Imbrication Angle (deg)	*P*	*T*	Shape
North margin	16	1.030 ± 0.011	0.033 ± 0.135	neutral
South margin	6	1.032 ± 0.006	0.274 ± 0.192	slightly oblate

[a]Imbrication angles, anisotropy, and shape parameters of samples from the dykes of Site 4, Lombo Gordo.

As a resume our data set suggests that the dominant magma flow pattern in dykes is lateral, away from the volcanic centers. In fact, 53 margins (out of the 66 margins from the 34 sampled dykes) show a normal magnetic fabric and 43 out of these margins yield a subhorizontal magmatic flow. In 12 dykes (five from São Jorge, five from São Miguel, and two from Santa Maria), the data for both margins are coincident. For Santa Maria the calculated magmatic flow is subhorizontal to oblique and no vertical or subvertical magmatic flow can be identified in any single dyke or margin.

Only three dykes from São Jorge (both margins of Jr7, plus the NE margin of Jr1 and the SW margin of Jr3) clearly exhibit a vertical magmatic flow, which, in these cases, takes place from top to bottom. We thus have no evidence of a direct feeding of the dykes from a continuous magma layer at depth. Rather, we interpret these results as indicating that magma was fed into the upper crust by magma injected in a horizontal or subhorizontal direction from volcanic centers inside the islands.

5.5. Indications of an External Dextral Shear Strain?

As previously pointed, at Site 4 on the eastern shore of São Miguel it was possible to obtain a dense sampling at both margins of nine dykes trending roughly E-W. The density contours of the k_3 axes of Site 4 (Figure 17) show that the imbrications angles at both margins are coherent but systematically display a slight difference in angle amplitude: along the northern margins a mean imbrication angle $\varphi_N = 16°$, while along the southern margins a mean imbrication angle $\varphi_S = 6°$ (Table 7). It is interesting to note that the degree of anisotropy P' at both margins is similar, but the shape parameter shows important differences between northern and southern margins of dykes at this site.

This asymmetrical fabric could be interpreted as the result of a shear displacement of the dyke walls during the magma injection [*Rochette et al.,* 1991; *Correa-Gomes et al.,* 2001; *Féménias et al.,* 2004]. Indeed, a theoretical symmetrical fabric model can be applied when a narrow dyke is injected in an isotropic strain field. However, if an anisotropic regional strain field or a horizontal strike slip is applied roughly parallel to the dyke strike during the final phases of dyke injection (with the magma flow arrested while still a viscous fluid), a corresponding shear should occur (that is a late-stage Couette flow superimposed on an overall laminar flow). The observed asymmetry in the fabric could thus result from the application of an external shear strain. In the Lombo Gordo dykes, the northern margins systematically display a higher imbrication angle and an almost neutral shape of the fabric, while the southern margins show smaller imbrication angles with a slightly oblate shape of the fabric. This asymmetrical magnetic fabric would be compatible with an external dextral shear coeval with the intrusion of the magma [*Correa-Gomes et al.,* 2001; *Féménias et al.,* 2004].

A similar asymmetrical distribution of imbrications also appears to occur at Site 5 (Faial da Terra) where the mean imbrication angle in the eastern margins is $\varphi_E = 34°$ and the mean imbrication in the western margins is $\varphi_W = 14°$. Nevertheless, the number of sampled dykes/margins at this site is relatively low, and we will not develop such analysis for this site.

6. Conclusions

The detailed study of magnetic properties of dykes from the Azores shows that, in this volcano-tectonic environment, they can be used to infer the fossilized flow pattern within the intrusive complex of this hot spot-related rift system. These dykes solidify at depth within the crust or as they crosscut the ground surface, acting as feeders for the extrusive lavas. They are thus essential in the crustal accretion of the Azores igneous crust.

AMS measurements allow us to conclude that the magmatic flow within these upper crustal dykes is predominantly horizontal or with a slight inclination, propagating away from the volcanic centers on the islands (Figure 16). There are some exceptions such as observed in a dyke from São Jorge where vertical

©2014. American Geophysical Union. All Rights Reserved.

(downward direction) flow is inferred and in dykes on the northern shore of Santa Maria yielding oblique flows of uncertain interpretation.

From these data we conclude that the magma forming the volcanic upper crust in the Azores is injected from a limited number of igneous centers, feeding dykes in a subhorizontal pattern which propagates away from these centers in agreement with the model of Figure 1.

In the light of these observations, it appears unnecessary to invoke the existence of a uniformly melting asthenosphere that would promote, either directly or indirectly, a general upward flow of magma through a deep magma layer as proposed in Iceland [*Bjornsson et al.,* 1979]. Instead, these results point toward a model of localized mantle melting with point sources feeding permanent upper crustal igneous centers with central magma chambers underlying central volcanoes. The magma stored in these chambers is then injected laterally into the crust as dykes by hydraulic-type fracturing of the magma chamber [*Geoffroy*, 1998; *Doubre and Geoffroy*, 2003]. These dykes would be injected parallel to the trend of the local principal horizontal stress, which is a combination of pressure fields around the magma chamber and gravitational and tectonic stresses [*Chevalier and Verwoerd,* 1988]. It is interesting to note that such a mechanism would account for the formation of São Jorge island which is made up of an elongated volcanic ridge and without any apparent crustal igneous center [*Hildenbrand et al.,* 2008]. As mentioned before, in São Jorge we obtain for the 120°–140° azimuth dykes a range of magmatic flows in opposite directions. One of the possibilities that may partly explain this result is an eventual change of the localization of magmatic sources or a migration of the volcanic activity [*Hildenbrand et al.,* 2008]. The lack of age determination of the studied dykes does not make possible to correlate the obtained directions with the ages of the dykes. Therefore, we tentatively propose that the inferred flow that is coming equally from the SE and from the NW, possibly reflect the existence of two-point source, one at the center of the island and the other offshore near its SE extremity.

Although we drilled most of the dykes that could be observed in the studied areas, we are fully aware of the limited amount of data in support of our model. However, our results are consistent with the overall volcano-tectonic pattern of the TRS which suggests that the volcano-tectonic configuration is highly segmented with localized melting zones at depth (see section 1.3). Finally, we suggest that a component of dextral shear with NW-SE trend is expressed in the igneous fabric of suitably oriented dykes, especially in those from the eastern and southeastern of São Miguel island (Site 4, Lombo Gordo, and Site 5, Faial da Terra). This hypothesis is in good agreement with present-day tectonics (see section 1.2) which would suggest that dextral shear existed since at least the Brunhes-Matuyama transition at 0.780 Ma (see section 2.2).

Acknowledgments
This study forms part of the PhD project of the first author. We greatly acknowledge Bernard Henry and Maxime le Goff for their support in the high field magnetic measurements performed at the "Observatoire de Magnétisme" at Saint-Maur, (IPGP, Paris), Charles Aubourg (Université de Pau) for fruitful discussions concerning composite magnetic fabrics and AARM measurements, and Cécile Doubre for her participation in the collection of samples on São Miguel and Santa Maria. We also warmly thank José Madeira and António Mateus from the Geological Department of the Faculty of Sciences of Lisbon, respectively, for providing helpful information on particular details of the geology of the Azores and for the use and interpretation of results from the Electron Probe Microanalyzer. This work was partially financed by project FCT: " IDL-LA0019-2015" and project REGENA PTDC/GEO-FIQ/3648/2012. M.S. N. Carpenter postedited the English style. We greatly thank M. Walter, W. Hastie, M. Petronis, and B. Henry for the useful comments and suggestions.

References

Abdel-Monem, A., L. Fernandez, and G. Boone (1975), K-Ar ages from the eastern Azores group (Santa Mafia, Miguel and the Formigas Islands), *Lithos, 8*, 247–254.

Arbaret, L., H. Diot, and J. L. Bouchez (1996), Shape fabrics of particles in low concentration suspensions: 2D analogue experiments and application to tiling in magma, *J. Struct. Geol.*, *15*, 941–950.

Asimow, P. D., and C. H. Langmuir (2003), The importance of water to oceanic mantle melting regimes, *Nature*, *421*(6925), 815–20, doi:10.1038/nature01429.

Aubourg, C., G. Giordano, M. Mattei, and F. Speranza (2002), Magma flow in sub-aqueous rhyolitic dykes inferred from magnetic fabric analysis (Ponza Island, W. Italy), *Phys Chem Earth*, *27*, 1263–1272.

Aubourg, C., G. Tshoso, B. L. Gall, H. Bertrand, and J. Tiercelin (2008), Magma flow revealed by magnetic fabric in the Okavango giant dyke swarm, Karoo igneous province, northern Botswana, *J. Volcanol. Geotherm. Res.*, *170*, 247–261, doi:10.1016/j.jvolgeores.2007.10.013.

Bjornsson, A., G. Johnsen, S. Sigurdson, G. Thorbergsson, and E. Tyggvason (1979), Rifting of the plate boundary in north Iceland 1975–1978, *J. Geophys. Res.*, *84*(B6), 3029–2038, doi:10.1029/JB084iB06p03029.

Bonati, E. (1990), Not so hot "hot spots" in the oceanic mantle, *Science*, *250*(4977), 107–111, doi:10.1126/science.250.4977.107.

Borradaile, G. J. (1988), Magnetic susceptibility, petrofabrics and strain, *Tectonophysics*, *156*, 1–20, doi:10.1016/0040-1951(88)90279-X.

Buforn, E., A. Udías, and M. A. Colombás (1988), Seismicity, source mechanisms and seismotectonics of the Azores-Gibraltar plate boundary, *Tectonophysics*, *152*, 89–118.

Burg, J.-P., J.-L. Bodinier, T. Gerya, R.-M. Bedini, F. Boudier, J.-M. Dautria, V. Prikhodko, A. Efimov, E. Pupier, and J.-L. Balanec (2009), Translithospheric mantle diapirism: Geological evidence and numerical modelling of the Kondyor zoned ultramafic complex (Russian Far-East), *J. Petrology*, *50*(2), 289–321, doi:10.1093/petrology/egn083.

Butler, R. (1992), *Paleomagnetism: Magnetic Domains to Geologic Terranes*, 238 pp., Blackwell Sci., Oxford, Boston, Mass.

Callot, J. P., and L. Geoffroy (2004), Magma flow in the East Greenland dyke swarm inferred from study of anisotropy of magnetic susceptibility: Magmatic growth of a volcanic margin, *Geophys. J. Int.*, *159*(2), 816–830, doi:10.1111/j.1365-246X.2004.02426.x.

Callot, J. P., and X. Guichet (2003), Rock texture and magnetic lineation in dykes: A simple analytical model, *Tectonophysics*, *366*, 207–222, doi:10.1016/S0040-1951(03)00096-9.

©2014. American Geophysical Union. All Rights Reserved.

Callot, J. P., L. Geoffroy, C. Aubourg, J. P. Pozzi, and D. Mege (2001), Magma flow directions of shallow dykes from the East Greenland volcanic margin inferred from magnetic fabric studies, *Tectonophysics*, *335*, 3–4, 313–329 doi.10.1016/S0040-1951(01)00060-9.
Canon-Tapia, E. (1996), Single-grain versus distribution anisotropy: A simple three-dimensional model, *Phys. Earth Planet. Inter.*, *9201*(94), 149–158.
Chadima, M., V. Cajz, and P. Týcová (2009), On the interpretation of normal and inverse magnetic fabric in dikes: Examples from the Eger Graben, NW Bohemian Massif, *Tectonophysics*, *466*(1–2), 47–63.
Chevalier, L., and W. Verwoerd (1988), A numerical model for the mechanical behavior of intraplate volcanoes, *J. Geophys. Res.*, *93*(B5), 2156–2202, doi:10.1029/JB093iB05p04182.
Correa-Gomes, L. C., C. R. Filho, C. J. Martins, and E. P. Oliveira (2001), Development of symmetrical and asymmetrical fabrics in sheet-like igneous bodies: The role of magma flow and wall-rock displacements in theoretical and natural cases, *J. Struct. Geol.*, *23*, 1415–1428.
Day, R., M. Fuller, and V. A. Schmidt (1977), Hysteresis properties of titanomagnetites: Grain-size and composition dependence, *Phys Earth Planet. Inter.*, *13*(4), 260–267, doi:10.1016/0031-9201(77)90108-x.
De Chabalier, J.-B., and J.-P. Avouac (1994), Kinematics of the Asal Rift (Djibouti) determined from the deformation of Fiaele Volcano, *Science*, *265*(5179), 1677–1681.
De Mets, C., R. G. Gordon, D. F. Argus, and S. Stein (1990), Current plate motions, *Geophy. J. Inter.*, *101*(2), 425–478.
Dosso, L., H. Bougault, C. Langmuir, C. Bollinger, O. Bonnier, and J. Etoubleau (1999), The age and distribution of mantle heterogeneity along the Mid-Atlantic Ridge (31–41°N), *Earth Planet. Sci. Lett.*, *170*, 269–286.
Doubre, C., and L. Geoffroy (2003), Rift-zone development around a plume-related magma centre on the Isle of Skye (Scotland): A model for stress inversions, *Terra Nova*, *15*, 230–237, doi:10.1046/j.1365-3121.2003.00494.x.
Dragoni, M., R. Lanza, and A. Tallarico (1997), Magnetic anisotropy produced by magma flow: Theoretical model and experimental data from Ferrar dolerite sills (Antarctica), *Geophys. J. Inter.*, *128*, 230–240.
Dunlop, D., and O. Özdemir (1997), *Rock Magnetism: Fundamentals and Frontiers*, 573 pp., Cambridge Univ. Press, Cambridge.
Durand, C., P. Gente, and O. Dauteuil (1995), Caractéristiques morphologiques des segments axiaux le long de la dorsale Médio-Atlantique (20°N–24°N), *C.R. Acad. Sci. Paris*, *320*, 411–418, Série IIa.
Elwood, B. B. (1978), Flow and emplacement direction determined for selected basaltic bodies using magnetic susceptibility anisotropy measurements, *Earth Planet. Sci. Lett.*, *41*, 254–264.
Féménias, O., H. Diot, T. Berza, A. Gauffriau, and D. Demaiffe (2004), Asymmetrical to symmetrical magnetic fabric of dikes: Paleo-flow orientations and paleo-stresses recorded on feeder-bodies from the Motru Dike Swarm (Romania), *J. Struct. Geol.*, *26*(8), 1401–1418, doi:10.1016/j.jsg.2003.12.003.
Feraud, G., I. Kaneoka, and J.-C. Allègre (1980), K/Ar ages and stress pattern in the Azores: Geodynamic implications, *Earth Planet. Sci. Lett.*, *46*(2), 275–286.
Feraud, G., H. U. Schmincke, J. Lietz, J. Gastaud, G. Pritchard, and U. Bleil (1981), New K-Ar ages, chemical analyses and magnetic data of rocks from the Islands of Santa Maria (Azores), Porto Santo and Madeira (Madeira Archipelago) and Gran Canaria (Canary Islands), *Bull. Volcanol.*, *44*(3), 359–375.
Ferré, E. C. (2002), Theoretical models of intermediate and inverse AMS fabrics, *Geophys. Res. Lett.*, *29*(7), 1127, doi:10.1029/2001GL014367.
Forjaz, V. H. (1980), Erupções históricas do sistema vulcânico Faial-Pico-Sao Jorge, Relatório Interno 01/80, Laboratório de Geociências e Tecnologia, S.R.C.I., Ponta Delgada, Açores, Portugal.
Gac, S., and L. Geoffroy (2005), Axial magnetic anomaly segmentation along the East-Greenland volcanic passive margin compared to magnetic segmentation of the Mid- Atlantic Ridge: A similar origin?, *Geophys. Res. Abstr.*, *7*, 07049. *S Ref-ID: 1607-7962/gra/EGU05-A-07049*.
Gaillot, P., M. D. Saint-Blanquat, and J. L. Bouchez (2006), Effects of magnetic interactions in anisotropy of magnetic susceptibility: Models, experiments and implications for igneous rock fabrics quantification, *Tectonophysics*, *418*, 3–19, doi:10.1016/j.tecto.2005.12.010.
Gente, P., R. A. Pockalny, C. Deplus, M. Maia, G. Ceuleneer, C. M. M. Cannat, and C. Laverne (1995), Characteristics and evolution of the segmentation of the Mid-Atlantic Ridge between 20°N and 24°N during the last 10 million years, *Earth Planet. Sci. Lett.*, *129*, 55–71.
Gente, P., J. Dyment, M. Maia, and J. Goslin (2003), Interaction between the Mid-Atlantic Ridge and the Azores hot spot during the last 85 Myr: Emplacement and rifting of the hot spot-derived plateaus, *Geochem. Geophys. Geosyst.*, *4*(10, 8514), doi:10.1029/2003GC000527.
Geoffroy, L. (1998), Diapirism and intraplate extension: Cause or consequence?, *C. R. Acad. Sci., Ser. IIa: Sci. Terre Planets*, *326*(4), 8050.
Geoffroy, L. (2005), Volcanic passive margins, *C. R. Geosci.*, *337*, 1395–1408, doi:10.1016/j.crte.2005.10.006.
Geoffroy, L., J. P. Callot, C. Aubourg, and M. Moreira (2002), Magnetic and plagioclase discrepancy in dykes: A new way to define the flow vector using magnetic foliation, *Terra Nova*, *14*(3), 183–190, doi:10.1046/j.1365-3121.2002.00412.x.
Geoffroy, L., C. Aubourg, J.-P. Callot, and L. Geoffroy (2007), Mechanisms of crustal growth in large igneous provinces: The north Atlantic province as a case study, *Geol. Soc. Am. Spec. Pap.*, *430*, 747-774, doi:10.1130/2007.2430(34).
Graham, J. W. (1954), Magnetic anisotropy, an unexploited petrofabric element, *Bull. Geol. Soc. Am.*, *65*, 1257–1258.
Grimison, N. L., and W.-P. Chen (1986), The Azores-Gibraltar Plate boundary: Focal mechanisms, depths of earthquakes, and their tectonic implications, *J. Geophys. Res.*, *91*(B2), 2029–2047, doi:10.1029/JB091iB02p02029.
Grommé, C. S., T. Wright, and D. Peck (1969), Magnetic properties and oxidation of iron-titanium oxide minerals in Alae and Makaopuhi Lava Lakes, Hawaii, *J. Geophys. Res.*, *74*(22), 5277–5293, doi:10.1029/JB074i022p05277.
Gudmundsson, A. (1986), Mechanical aspects of postglacial volcanism and tectonics of the Reykjanes Peninsula, southwest Iceland, *J. Geophys. Res.*, *91*(B12), 12,711–12,721, doi:10.1029/JB091iB12p12711.
Gudmundsson, A. (1990), Emplacement of dikes, sills and crustal magma chambers at divergent plate boundaries, *Tectonophysics*, *176*3–4, 257-275, doi:10.1016/0040-1951(90)90073-H.
Hargraves, R. B., and D. Johnson (1991), Distribution anisotropy: The cause of AMS in igneous rocks?, *Geophys. Res. Lett.*, *18*(12), 2193–2196, doi:10.1029/91GL01777.
Henry, B., and M. Le Goff (1995), Application de l'extension bivariate de la statistique de Fisher aux données d'anisotropie de susceptibilité magnétique: Intégration des incertitudes de mesure sur l'orientation des directions principales, *C. R. Acad. Sci. Paris, 320* IIa, 1037–1042.
Hildenbrand, A., P. Madureira, F. Ornelas, I. Cruz, B. Henry, and P. Silva (2008), Multi-stage evolution of a sub-aerial volcanic ridge over the last 1.3 Myr: S. Jorge Island, Azores triple junction, *Earth Planet. Sci. Lett.*, *273*, 289–298, doi:10.1016/j.epsl.2008.06.041.
Hildenbrand, A., F. O. Marques, A. C. G. Costa, A. L. R. Sibrant, P. F. Silva, B. Henry, J. M. Miranda, and P. Madureira (2012), Reconstructing the architectural evolution of volcanic islands from combined K/Ar, morphologic, tectonic, and magnetic data: The Faial Island example (Azores), *J. Volcanol. Geotherm. Res.*, *241-242*, 39–48, doi:10.1016/j.jvolgeores.2012.06.019.
Hirn, A., H. Haessler, P. Hoang-Trong, G. Wittlinger, and L. A. MendesVictor (1980), Aftershock sequence of the January 1st, 1980, earthquake and present-day tectonics in the Azores, *Geophys. Res. Lett.*, *7*(7), 501–504, doi:10.1029/GL007i007p00501.

©2014. American Geophysical Union. All Rights Reserved.

Hirn, A., J.-C. Lépine, and M. Sapin (1993), Triple junction and ridge hotspots: Earthquakes, faults, and volcanism in Afar, the Azores, and Iceland, *J. Geophys. Res.*, *98*(B7), 11,995–12,001, doi:10.1029/93JB00373.
Hrouda, F. E. K. (1982), Magnetic anisotropy of rocks and its application in geology and geophysics, *Geophys. Surv.*, *5*, 37–82.
Hrouda, F. E. K. (2002), Low field variation of magnetic susceptibility and its effect on the anisotropy of magnetic susceptibility of rocks, *Geophys. J. Int.*, *150*, 715–723.
Ildefonse, B., P. Launeau, J. Bouchez, and A. Fernandez (1992), Effect of mechanical interactions on the development of shape preferred orientations: A two-dimensional experimental approach, *J. Struct. Geol.*, *14*(1), 73–83.
Jeffery, G. B. (1922), The motion of ellipsoidal particles immersed in a viscous fluid, *Proc. R. Soc. London*, *102*(715), 161–179, doi:10.1098/rspa.1922.0078.
Jelinek, W. I. T. (1978), Statistical processing of anisotropy of magnetic susceptibility measured on groups of specimens, *Stud. Geophys. Geod.*, *22*, 50–62.
Jelinek, W. I. T. (1981), Characterization of magnetic fabric of rocks, *Tectonophysics*, *79*(3-4), T63–T67.
Johnson, C. L., J. R. Wijbrans, C. G. Constable, J. Gee, H. Staudigel, L. Tauxe, V. Forjaz, and M. Salgueiro (1998), $^{40}Ar/^{39}Ar$ Ar ages and paleomagnetism of São Miguel lavas, Azores, *Earth Planet. Sci. Lett.*, *160*, 637–649.
Khan, M. A. (1962), The anisotropy of magnetic susceptibility of some igneous and metamorphic rocks, *J. Geophys. Res.*, *67*(7), 2873–2885, doi:10.1029/JZ067i007p02873.
Knight, M. D., and G. P. L. Walker (1988), Magma flow directions in dikes of the Koolau Complex, Oahu, determined from magnetic fabric studies, *J. Geophys. Res.*, *93*(B5), 4301, doi:10.1029/JB093iB05p04301.
Launeau, P., and P.-Y. F. Robin (1996), Fabric analysis using the intercept method, *Tectonophysics*, *267*, 91–119.
Lin, J., G. Purdy, H. Schouten, J. C. Sempere, and C. Zervas (1990), Evidence from gravity data for focused magmatic accretion along the Mid-Atlantic Ridge, *Nature*, *344*(6267), 627–632.
Lourenço, N., J. M. Miranda, J. F. Luis, A. Ribeiro, L. A. M. Victor, J. Madeira, and H. D. Needham (1998), Morpho-tectonic analysis of the Azores Volcanic Plateau from a new bathymetric compilation of the area, *Mar. Geophys. Res.*, *20*, 141–156.
Luis, J. F., and J. M. Miranda (2008), Reevaluation of magnetic chrons in the North Atlantic between 35°N and 47°N: Implications for the formation of the Azores triple junction and associated plateau, *Atlantic*, *113*, 1–12, doi:10.1029/2007JB005573.
Luis, J. F., and M. C. Neves (2006), The isostatic compensation of the Azores Plateau: A 3D admittance and coherence analysis, *J. Volcanol. Geotherm. Res.*, *156*(1-2), 10–22, doi:10.1016/j.jvolgeores.2006.03.010.
Luis, J. F., J. M. Miranda, A. Galdeano, and P. Patriat (1989), Constraints on the structure of the Azores spreading center from gravity data, *Mar. Geophys. Res.*, *20*, 157–170.
Luís, J. F., J. M. Miranda, A. Galdeano, P. Patriat, J. C. Rossignol, and L. A. Mendes-Victor (1994), The Açores triple junction evolution since 10 Ma from an aeromagnetic survey of the Mid-Atlantic, *Earth Planet. Sci. Lett.*, *125*, 439–459.
Macdonald, K. C., P. J. Fox, L. J. Perram, M. F. Eisen, R. M. Haymon, S. P. Miller, S. M. Carbotte, M.-H. Cormier, and A. N. Shor (1988), A new view of the mid-ocean ridge from the behaviour of ridge-axis discontinuities, *Nature*, *335*, 217–225, doi:10.1038/335217a0.
Madeira, J., and A. Brum (2003), Active tectonics and first paleoseismological results in Faial, Pico and S. Jorge Islands (Azores, Portugal), *Ann. Geophys.*, *46*(5), 733–761.
Madeira, J., A. Serralheiro, S. A. Monge, and C. F. Rodrigues (1998), Radioacarbon ages of recent volcanic events from the Island of S Jorge Azores, *Com. Inst. Geol. Min.*, *84*(1), 189–192.
McKenzie, D., and J. Morgan (1969), Evolution of triple junctions, *Nature*, *224*, 125–133, doi:10.1038/224125a0.
Miranda, J. M., L. A. M. Victor, J. Z. Simões, J. F. Luis, L. Matias, H. Shimamura, H. Shiobara, H. Nemoto, H. Mochizuki, and A. Hirn (1998), Tectonic setting of the Azores Plateau deduced from a OBS survey, *Mar. Geophys. Res.*, *20*, 171–182.
Moreira, M., R. Doucelance, M. Kurz, B. Dupré, and C. J. Allègre (1999a), Helium and lead isotope geochemistry of the Azores archipelago, *Earth Planet. Sci. Lett.*, *169*, 189–205.
Moreira, M., L. Geoffroy, and J. P. Pozzi (1999b), Ecoulement magmatique dans les dykes du point chaud des Açores: Etude préliminaire par anisotropie de susceptibilité magnétique (ASM) dans l'île de San Jorge, *C. R. Acad. Sci., Ser. IIa: Sci. Terre Planets,*, *329*(1), 15–22, doi:10.1016/S1251-8050(99)80222-5.
Özdemir, Ö. (1987), Inversion of titanomaghemites, *Phyis. Earth Planet. Inter.*, *46*(June), 184–196.
Paquet, F., O. Dauteuil, E. Hallot, and F. Moreau (2007), Tectonics and magma dynamics coupling in a dyke swarm of Iceland, *J. Struct. Geol.*, *29*(9), 1477–1493, doi:10.1016/j.jsg.2007.06.001.
Petronis, M. S., A. Delcamp, and B. van Wyk de Vries (2013), Magma emplacement into the Lemptégey scoria cone (Chaîne des Puys, France) explored with structural, anisotropy of magnetic susceptibility and Paleomagnetic data, *Bull. Volcanol.*, *75*(10), 753.
Philpotts, A. R., and D. E. Philpotts (2007), Upward and downward flow in a camptonite dike as recorded by deformed vesicles and the anisotropy of magnetic susceptibility (AMS), *J. Volcanol. Geotherm. Res.*, *161*, 81–94, doi:10.1016/j.jvolgeores.2006.11.006.
Potter, D. K., and A. Stephenson (1988), Single-domain particles in rocks and magnetic fabric analysis Geophysical Research Letters, *Geophys. Res. Lett.*, *15*(10), 1097–1100, doi:10.1029/GL015i010p01097.
Rochette, P., and C. Aubourg (1999), Is this magnetic fabric normal? A review and case studies in volcanic formations, *Tectonophysics*, *307*, 219–234.
Rochette, P., L. Jenatton, C. Dupuy, F. Boudier, and I. Reuber (1991), Diabase dykes emplacement in the Oman ophiolite: A magnetic fabric study with reference to geochemistry, in *Ophiolite Genesis and Evolution of the Oceanic Lithosphere*, edited by T. Peters, A. Nicolas, and R. G. Coleman, pp. 55–82, Kluwer, Dordrecht, Netherlands.
Rochette, P., M. Jackson, and C. Aubourg (1992), Rock magnetism and the interpretation of anisotropy of magnetic susceptibility, *Rev. Geophys.*, *30*(3), 209–226, doi:10.1029/92RG00733.
Schaefer, B. F., S. Turner, I. Parkinson, N. Rogers, C. Hawkesworth, E. Sciences, W. Hall, and M. Keynes (2002), Evidence for recycled Archaean oceanic mantle lithosphere in the Azores plume, *Nature*, *420*, 304–307, doi:10.1038/nature01172.
Searle, R. (1980), Tectonic pattern of the Azores spreading centre and triple junction, *Earth Planet. Sci. Lett.*, *51*(2), 415–434.
Serralheiro, A., and J. Madeira (1993), Stratigraphy and geochronology of Santa Maria Island (Azores), *Açoreana*, *7*(4), 575–592.
Serralheiro, A., C. A. M. Alves, V. H. Forjaz, and B. Rodrigues (1987), Carta vulcanológica dos Açores: Ilha de Santa Maria. *Edição do Serv. Reg. Protecção Civil (Região Autónoma dos Açores)*, Ponta Delgada, 1ª ed., 2 folhas.
Silva, P. F., B. Henry, F. O. Marques, A. Hildenbrand, P. Madureira, C. A. Mériaux, and Z. Kratinová (2012), Palaeomagnetic study of a subaerial volcanic ridge (São Jorge Island, Azores) for the past 1.3 Myr: Evidence for the Cobb Mountain subchron, volcano flank instability and tectonomagmatic implications, *Geophysic. J. Inter.*, *188*(3), 959–978, doi:10.1111/j.1365-246X.2011.05320.x.
Silva, P. F., F. O. Marques, M. Machek, B. Henry, A. M. Hirt, Z. Roxerová, P. Madureira, and S. Vratislav (2014), Evidence for non-coaxiality of ferrimagnetic and paramagnetic fabrics, developed during magma flow and cooling in a thick mafic dyke, *Tectonophysics*, *629*, 155–164, doi:10.1016/j.tecto.2014.04.017.

©2014. American Geophysical Union. All Rights Reserved.

Silveira, G., E. Stutzmann, A. Davaille, J.-P. Montagner, L. Mendes-Victor, and A. Sebai (2006), Azores hotspot signature in the upper mantle, *J. Volcanol. Geotherm. Res.*, doi:10.1016/j.jvolgeores.2006.03.022.

Soriano, C., E. Beamud, and M. Garcés (2008), Magma flow in dikes from rift zones of the basaltic shield of Tenerife, Canary Islands: Implications for the emplacement of buoyant magma, *J. Volcanol. Geotherm. Res.*, *173*, 55–68, doi:10.1016/j.jvolgeores.2008.01.007.

Stacey, F. D. (1960), Magnetic anisotropy of igneous rocks, *J. Geophys. Res.*, *65*(8), 2429–2442, doi:10.1029/JZ065i008p02429.

Storetvedt, K. M., A. Serraiheiro, M. Moreira, and M. C. Abranches (1989), Magnetic structure and evolution of the island of Santa Maria, Azores, *Phys. Earth Planet. Inter.*, *58*, 228–238.

Tarling, D. H., and F. Hrouda (1993), *The Magnetic Anisotropy of Rocks*, 217 pp., Chapman and Hall, London.

Tauxe, L, S. K. Banerjee, R. F. Butler, and R. van der Voo (2012) *Essentials of Paleomagnetism*, 2nd web ed. [Avaliable at http://magician.ucsd.edu/Essentials_2/WebBook2.html.]

Tolstoy, M., A. J. Harding, J. A. Orcutt, M. Tolstoy, A. J. Harding, and J. A. Orcutt (1993), Crustal thickness on the Mid-Atlantic Ridge: Bull's eye gravity anomalies and focused accretion, *Science*, *262*(October), 726–729.

Vlastélic, I., H. Bougault, and L. Dosso (2002), Heterogeneous heat production in the Earth's upper mantle: Blob melting and MORB composition, *Earth Planet. Sci. Lett.*, *199*(1-2), 157–172.

Widom, E., and J. Farquhar (2003), Oxygen isotope signatures in olivines from Sao Miguel basalts (Azores): Implications for crustal and mantle processes, *Chem. Geol.*, *193*, 237–255.

Wright, T. J., F. Sigmundsson, C. Pagli, M. Belachew, I. J. Hamling, B. Brandsdottir, and D. Keir (2012), Geophysical constraints on the dynamics of spreading centres from rifting episodes on land, *Nat. Geosci.*, *5*(4), 242–250, doi:10.1038/ngeo1428.

Yang, T., Y. Shen, and S. Van Der Lee (2006), Upper mantle structure beneath the Azores hotspot from finite-frequency seismic tomography, *Earth Planet. Sci. Lett.*, *250*, 11–26, doi:10.1016/j.epsl.2006.07.031.

©2014. American Geophysical Union. All Rights Reserved.